The material budget of the ATLAS Inner Detector

Inner Detector Note INDET-NO-207

1 Introduction

At the time of the approval of the ATLAS Inner Detector Technical Design Report, the LHCC requested a follow up report on the material budget of the detector, to be presented with the Pixel sub-system TDR[11-1]. This report details the present material budget and the changes made since the original ID TDR. In the technical sections, (3 to 9), detailed comparisons are made between the present engineering designs and those presented in the ID TDR [11-2]. In Section 10, comparisons are made between the layout used for the performance simulations (known as 97-6) presented in [11-3] and the present layout[1]. Layout 97-6 described the engineering design of the TDR, and care was taken to make conservative estimates of the material for items where the design was not complete.

The principle difficulty caused by the ID material is a deterioration in the performance of the Inner Detector itself and of the electromagnetic calorimeter. These effects have been documented in detail in the Performance volumes of the ID and Calorimeter TDR's and more recently in the studies summarised in [11-3] and Section 12. These studies, already shown to the LHCC referees, were based on layout 97-6. The main effect on the ID is to degrade the pattern recognition as low energy pions interact. In the worst case, for pions with a p_T of 1 GeV, the reconstruction efficiency drops to 89%. In addition, tracks from photon conversions limit the light-quark jet rejection from vertexing. However the rejection remains high at 80, with a b-tagging efficiency of 50%, so the physics performance goals can nevertheless be met.

The calorimeter resolution suffers because of tails created by electromagnetic interactions in the material. The contribution made by material to the tails is strongly radially dependent. For example, the total contribution of the TRT material is smaller than that from a single precision layer, because of the short lever arm between the TRT material and the calorimeter. The impact of material in services has therefore been minimised by routing, wherever possible, the services to the outer radius of the detector by the shortest route. A comparison of the effect on the calorimeter performance for layout 97-6 and the present one is given in Section 2. The effect of these tails on the ATLAS physics potential remains small. For example, the presence of all of the ID material reduces the acceptance for H-> $\gamma\gamma$ by 3.8% to 80%. Similarly, while 89% of H-> 4e are reconstructed, 9% are lost from the mass peak because of tails in the resolution, leaving an acceptance of 86.2%. The effect is largest for this channel because any efficiency and resolution losses appear to the fourth power.

The LHCC ATLAS referees were sent a report [11-4] in August 1997, detailing the actions in progress and planned to optimise the material budget of the ID further. The Committee also requested a status report at the time of the pixel TDR, which is presented here.

1. The simulations presented in the ID TDR were made with an earlier version of the detector, since the simulation layout was frozen some 6 months before the TDR was completed.

2 Changes in the Material Distribution

In this section a comparison is made between the present simulation, which has been updated to reflect the current engineering design, and layout 97-6, which was used for the performance simulations of the effects of material [11-3].

The material in layout 97-6 is shown as a function of pseudo-rapidity |η| in Figure 2-1, while the latest

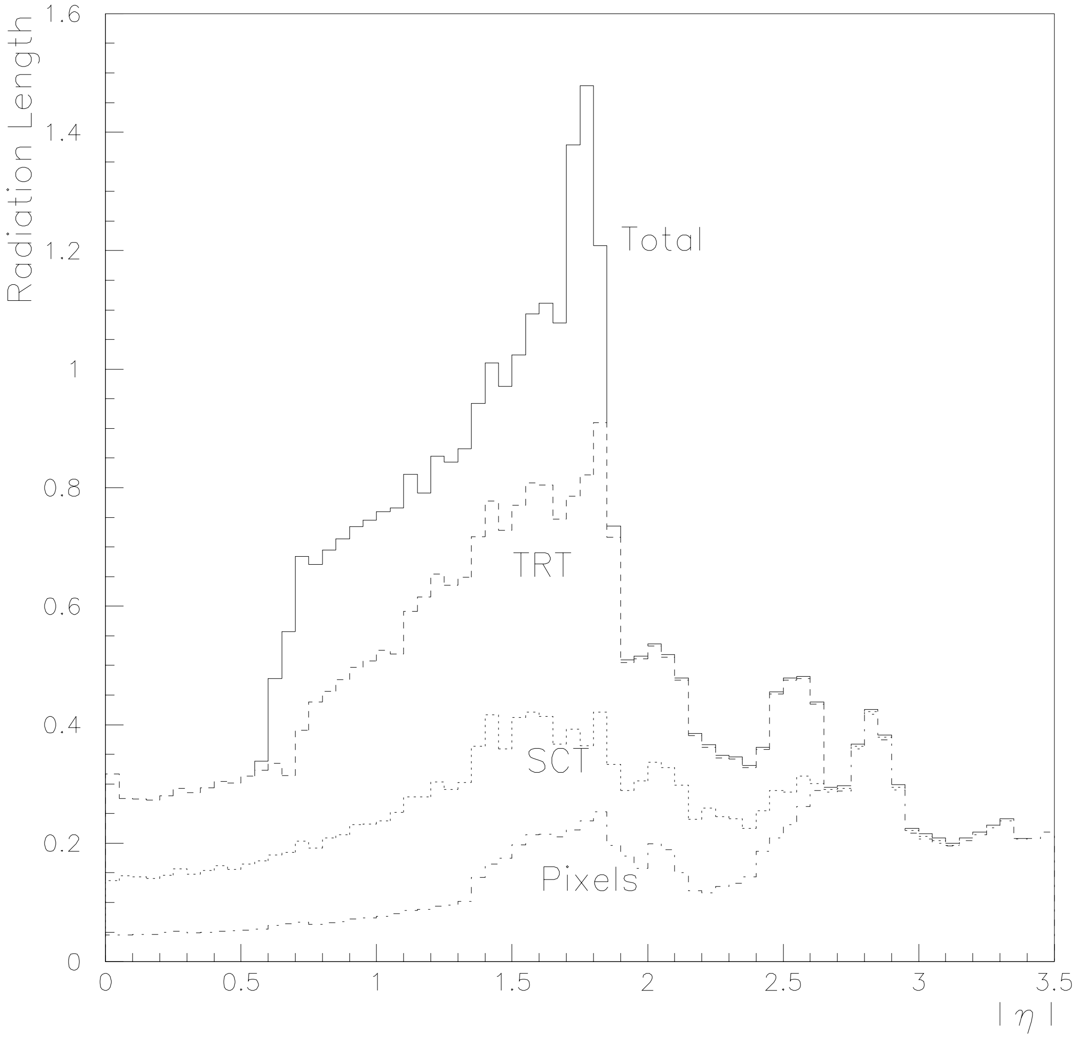

Figure 2-1 Material distribution of the ID vs |η| for the TDR design (layout 97-6). The pixel band includes beam pipe and local supports and services, the SCT band includes local supports and services, and the top band includes all other services and supports.

estimate is shown in Figure 2-2. The difference between them is shown in Figure 2-3.

The individual distributions for the 3 sub-systems and for the services in the barrel/end-cap crack and outside of the ID sensitive volume are shown in Figures 2-4 to 2-6 for layout 97-6, the present design and the difference between them respectively.

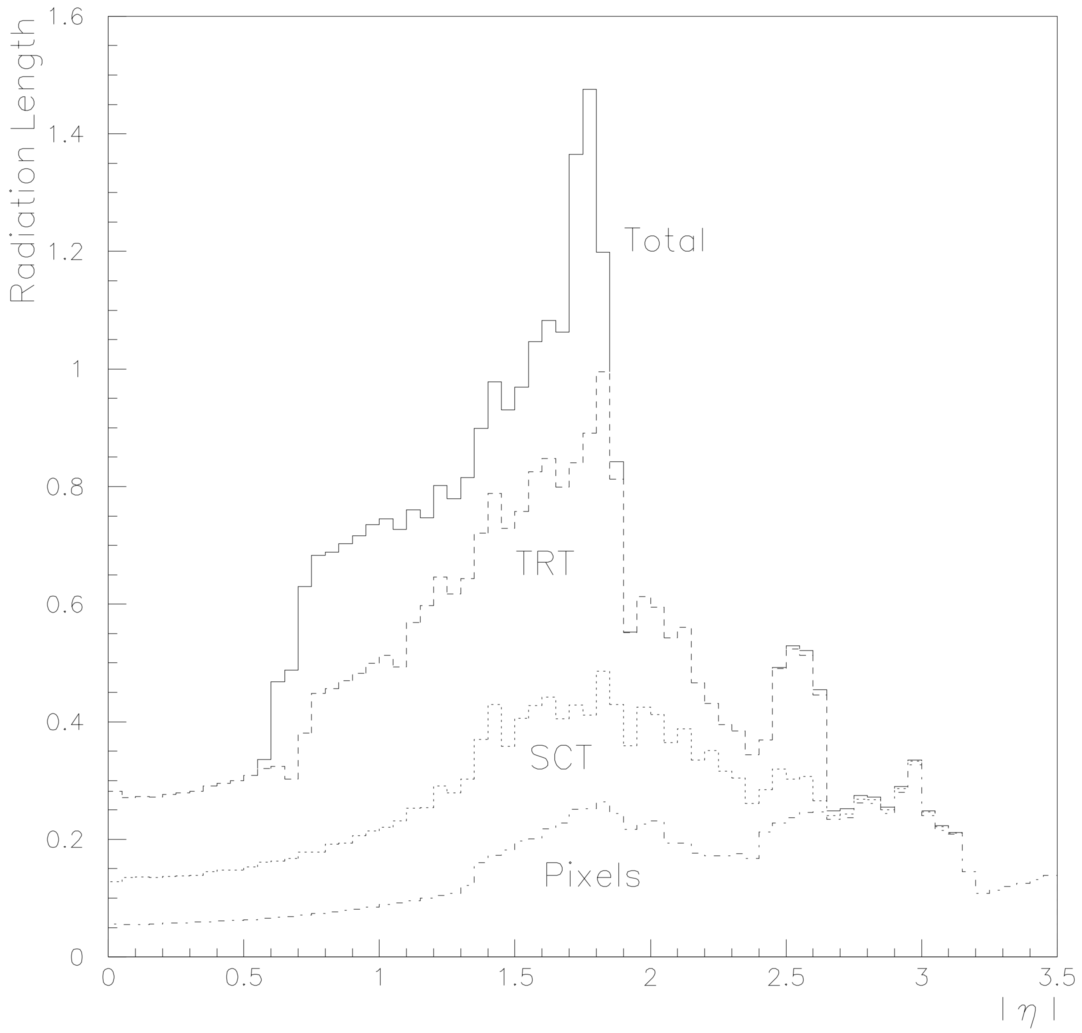

Figure 2-2 Material distribution of the ID vs |η| for the present engineering design. The pixel band includes beam pipe and local supports and services, the SCT band includes local supports and services, and the top band includes all other services and supports.

Table 2-1 shows the results of a study of low energy tails in the calorimeter in the worst case, for electrons with E_T = 10 GeV at η of 1.2, taken from [11-3]. It should be emphasised that the real effect on the physics performance of the calorimeter is much smaller, as illustrated by the figures quoted in Section 1. However, the long task of resimulating physics events throughout the detector has not been repeated. Instead, a simple scaling of the material present at this particular η allows an estimate to be made of the effect on the calorimeter of the changes for this case. It is seen that at this particular η point the tails in the calorimeter have been reduced.

The efforts made since last year have resulted in a stable total tracker material budget, in spite of increases in some items forced by the needs of access and maintenance. The distribution has shifted to higher |η|. The present estimates include items which were either poorly estimated or not foreseen at the time of the TDR, mostly at high radius, while savings have been made in the active region of the detector. Accordingly, a small reduction in the impact of the material on the tracking and EM calorimeter performance is expected.

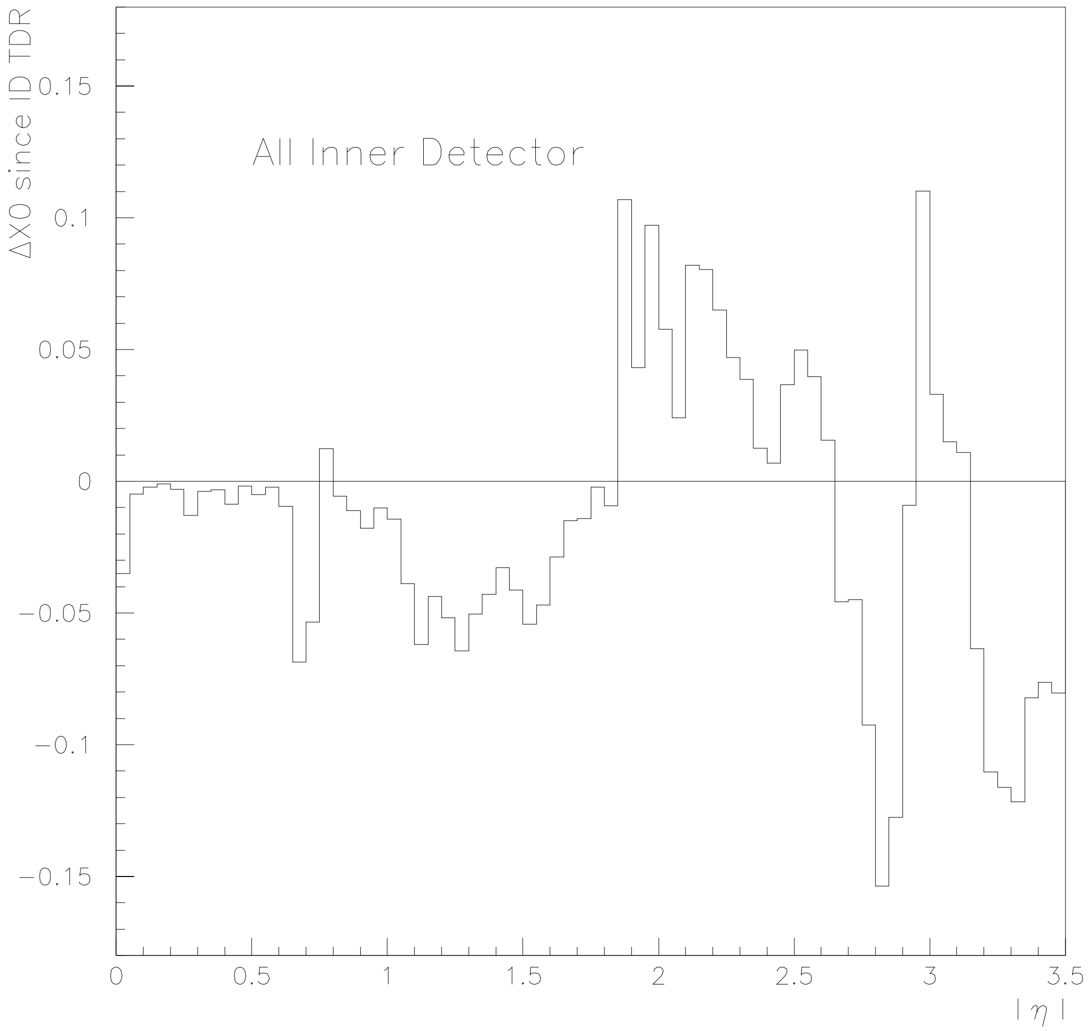

Figure 2-3 Change in the ID material distribution vs |η| from layout 97-6.

3 Layout

The layout of the ID has changed only slightly since the TDR was submitted. The main change is in the layout of the pixel disks, moving from 4 to 5 smaller disks per end-cap. The TDR layout is shown in Figure 3-1, and the new layout in Figure 3-2.

The effect of the layout changes on the material distribution is small, and is detailed in the sections below.

The Collaboration considered whether a reduction in the number of precision layers in the ID would produce a more optimal overall performance for ATLAS, by reducing the material in the ID (and hence the calorimeter resolution tails) without degrading the ID performance unacceptably. Three layouts were compared: the TDR design with 7 precision layers, including the pixel B-layer; a layout with only 3 SCT strip layers; and a layout with only 2 pixel layers. The results of the study are given in detail in [11-3], and a summary of this note is included in Section 12. The study concluded that while the EM calorimeter performance was slightly improved in the reduced layouts, the tracking performance was significantly degraded in b-tagging, Level-2 triggering, and K^0_S reconstruction. The uncertainties in the actual

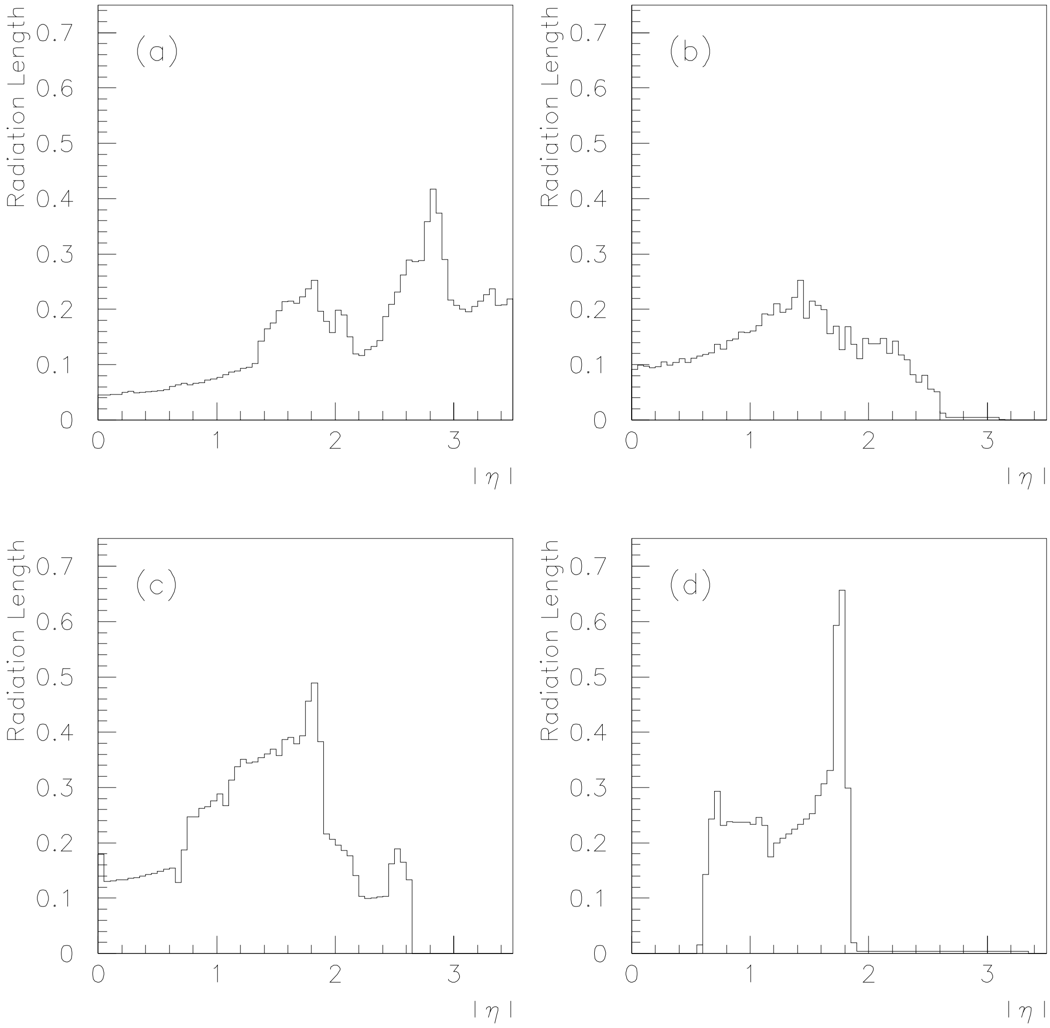

Figure 2-4 The material in the TDR design (layout 97-6) vs |η| for a) the pixels and beam-pipe, b) the SCT, c) the TRT and d) services and supports in the barrel/end-cap crack and outside of the ID sensitive volume.

performance in the presence of pile-up and after radiation damage were also a concern. Accordingly the Collaboration agreed that the baseline layout have 7 layers, including the pixel B-layer.

4 Cooling

On the 18th and 19th of September 1997, ATLAS held an internal review of the proposed non-cryogenic cooling systems of the experiment. This review, while wider in scope than the ID alone, fulfilled the function of the ID cooling review proposed in the action plan on material, and scheduled for the same date. The review committee included non-ATLAS cooling experts.

Among the general conclusions of the review is included:

"*Inert fluor should replace water for use in the cooling systems for the different sub- detectors*"

and

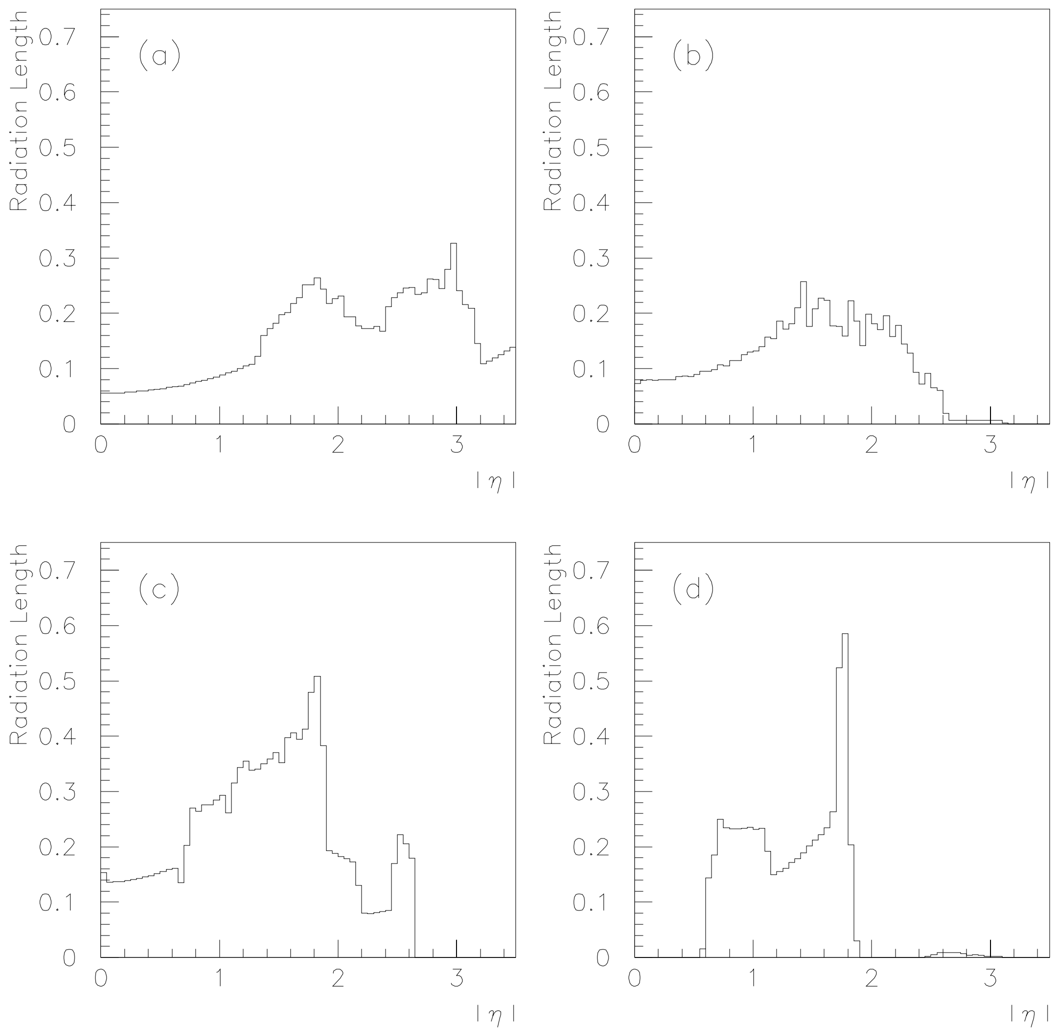

Figure 2-5 Material vs |η| for a) pixels and beam-pipe, b) SCT, c) TRT and d) services and supports in the barrel/end-cap crack and outside of the ID sensitive volume, as implemented in the current simulation program.

"*Leakless systems should be limited in use to applications where access for an intervention is difficult and where the consequences of a leak could be material damage to electrical components of detectors. These applications are typically inside the experiment*".

The first conclusion was motivated by the risk of damage to the detector by water leakage, especially to expensive electronics. The second conclusion was motivated by the general technical difficulties associated with sub-atmospheric pressure operation, in particular the limitations imposed by the small pressure drops available. In the case of the proposed binary ice system for the SCT and pixel sub-systems of the ID, this leads to the use of larger diameter pipework with consequent difficulties for the service routings in the confined space of the calorimeter cryostat.

The specific conclusions of the committee with respect to the SCT/pixel cooling were:

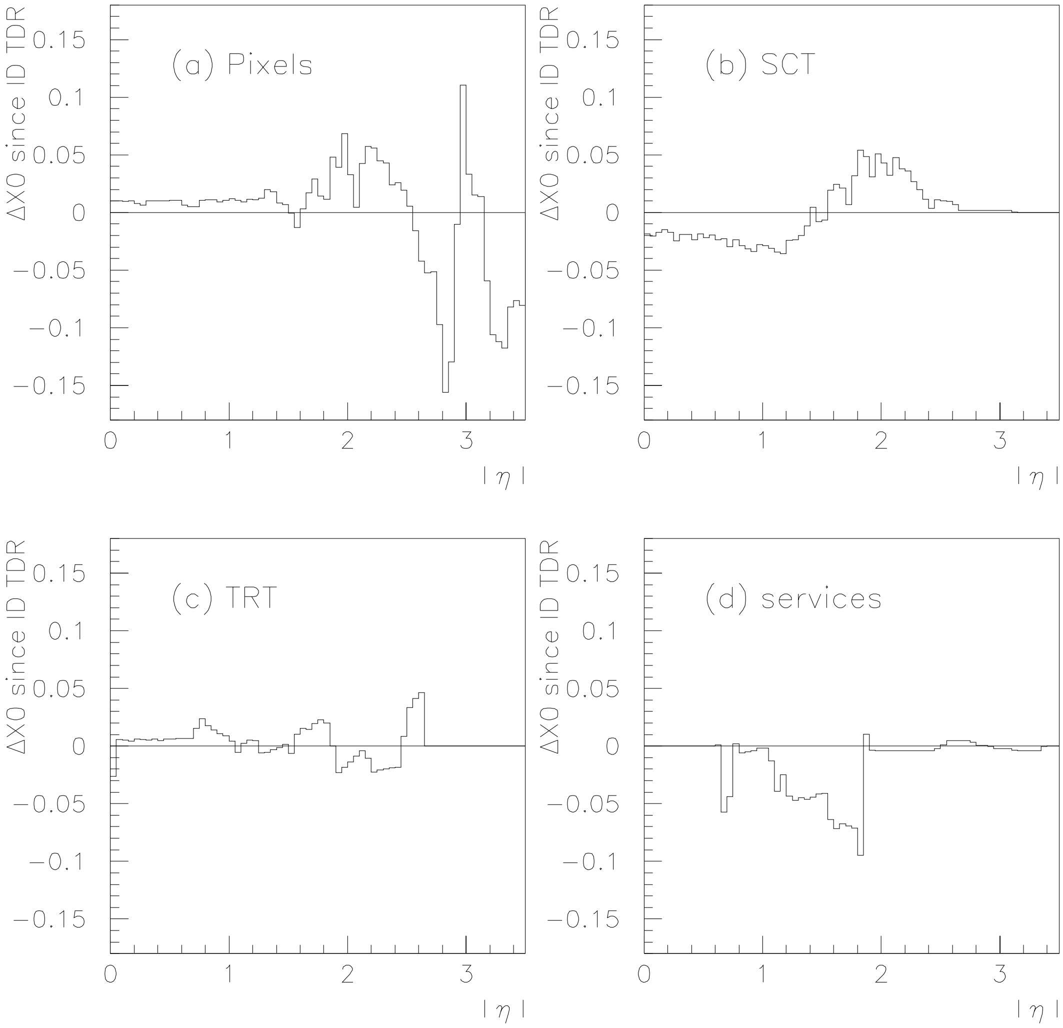

Figure 2-6 Change in material vs |η| for a) pixels, b)SCT, c) TRT and d) services and supports in the barrel/end-cap crack and outside of the ID sensitve volume, since the ID TDR (layout 97-6).

"*The committee believes that both binary ice and evaporative systems could perform the cooling task. However, when taking into account all the system aspects, they have a distinct preference for the evaporative system for the following reasons*:

- *it has a lower material budget*
- *the cooling medium is much safer*
- *the consequences of a leak are less drastic*
- *there are less components so reliability should be higher*
- *the routing of pipes is simpler and more likely to fit in the available space."*

For the TRT cooling, the committee approved of the use of carbon dioxide gas cooling in the end-cap wheels, but recommended that the pressurised water system used to cool the straws and electronics be replaced by a pressurised fluorinert.

Table 2-1 Low-energy tails in the EM calorimeter for 10 GeV p_T electrons at η=1.2 averaged over the longitudinal vertex spread.

	TDR Design	Present Design	TDR Design	Present Design
Source of tail	Radiation length at η=1.2 (%X_0)		% of electrons in low-energy tail	
Beam pipe	0.51	0.51	0.5	0.5
Pixel B-Layer	2.60	3.03	2.2	2.6
Pixel barrel 1	2.79	3.30	2.3	2.7
Pixel barrel 2	2.87	2.96	2.2	2.3
Pixel support	0.80	0.90	0.4	0.4
SCT Barrel 3	4.44	3.49	2.5	2.0
SCT Barrel 4	4.40	3.55	2.2	1.8
SCT Barrel 5	4.44	3.59	1.9	1.5
SCT services	10.00	9.55	2.4	2.3
TRT entrance	3.23	4.62	0.5	0.7
TRT detector	13.26	9.56	0.9	0.6
Outer services	32.33	32.89	1.0	1.0
TOTAL	**81.67**	**77.95**	**19.2 ± 0.6**	**18.4**

Since this review, the cooling work has focussed on the implementation of these recommendations. For the TRT system, the main problem under investigation is whether the relatively high Reynolds number required for the use of a low specific heat fluid will cause problems from vibrations. For the SCT/pixel systems, the tests have focussed on questions of vapour flow through the complex pipework required in the disk-geometry detectors, and on the behaviour of manifolded cooling in the presence of a failure of one cooling channel. Successful tests with manifolded pixel barrel staves and pixel disks in various geometries allow evaporative C_4F_{10} to be adopted as the baseline in this sub-system. Initial tests with a fully powered SCT stave have also given positive results, and construction of a SCT disk testbed is under way. This testbed will consist of a full-scale SCT disk, equipped with different geometry cooling channels in each of four quadrants. A large environmental box is being built to contain it, together with an enlarged data aquisition system. The tests will be carried out in cooperation with the CERN-wide cooling group set up recently to coordinate developments for all LHC experiments.

The use of liquid C_4F_{10} in the TRT implies a very small increase in material from the coolant, and possible increases if high pressure connectors are needed, but not in a critical region. A comparison of the material in the TRT compared to the situation at the time of the TDR is given in detail in Section 6.

For this report, the use of evaporative C_4F_{10} is assumed in the SCT, with a modularity of 8 delivery/recovery pipes per barrel layer, and 4 per disk. The aluminium delivery pipes are between 2 and 4 mm diameter, and the vapour recovery pipes are between 6 and 15 mm diameter, compared to 11 to 15 mm diameter for the binary ice option. This leads to savings in the barrel end-flange region, along the cryostat wall and at the outer boundary of the SCT end-cap region. The net change in material from this change is shown in the tables for the SCT and pixel detector systems, and is plotted in Section 9, including the effect of changes to the pipework routing. Test rigs are now under construction, which will also allow the final modularity of the system pipework to be chosen.

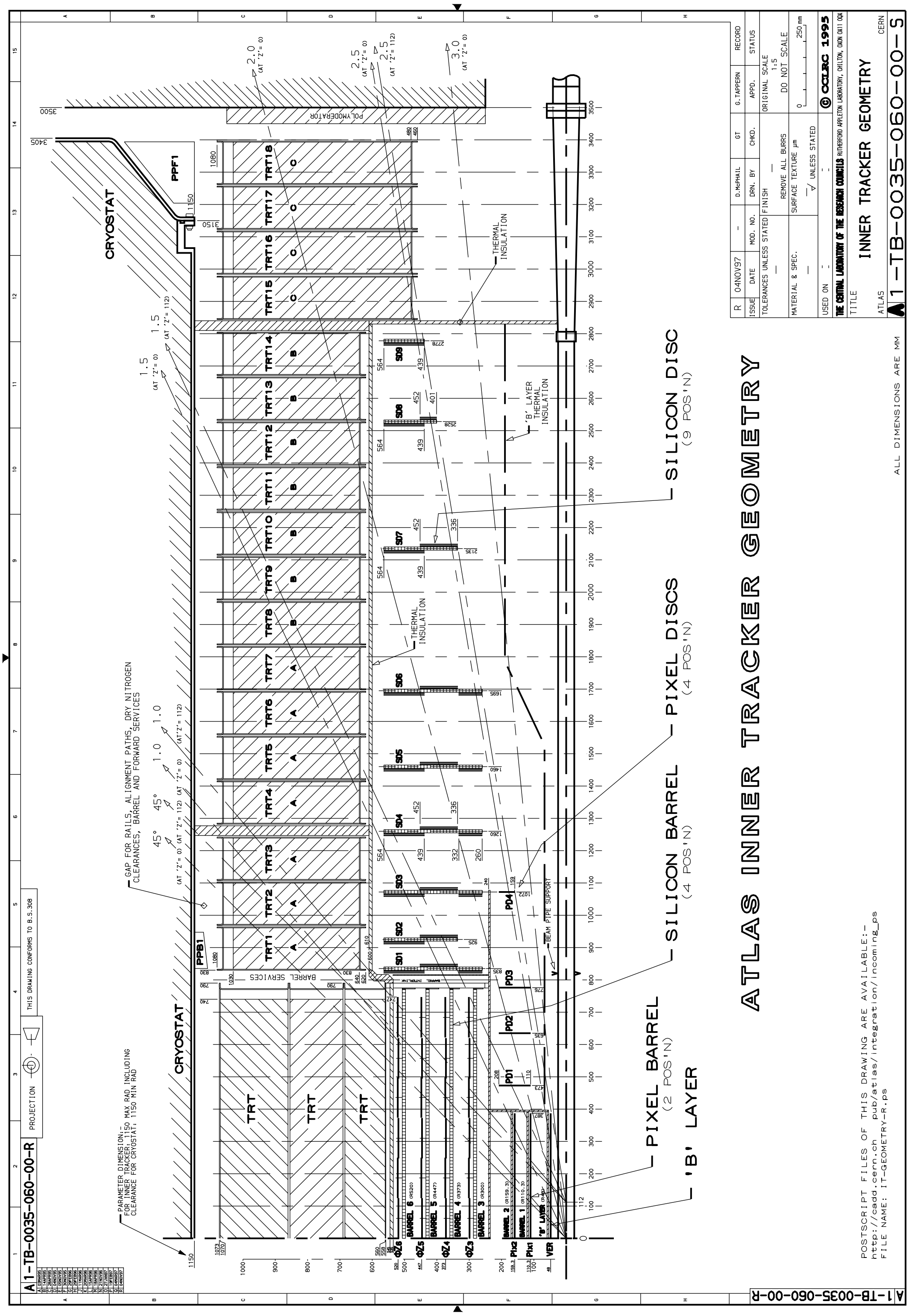

Figure 3-1 Layout of Inner Detector at the time of the ID TDR.

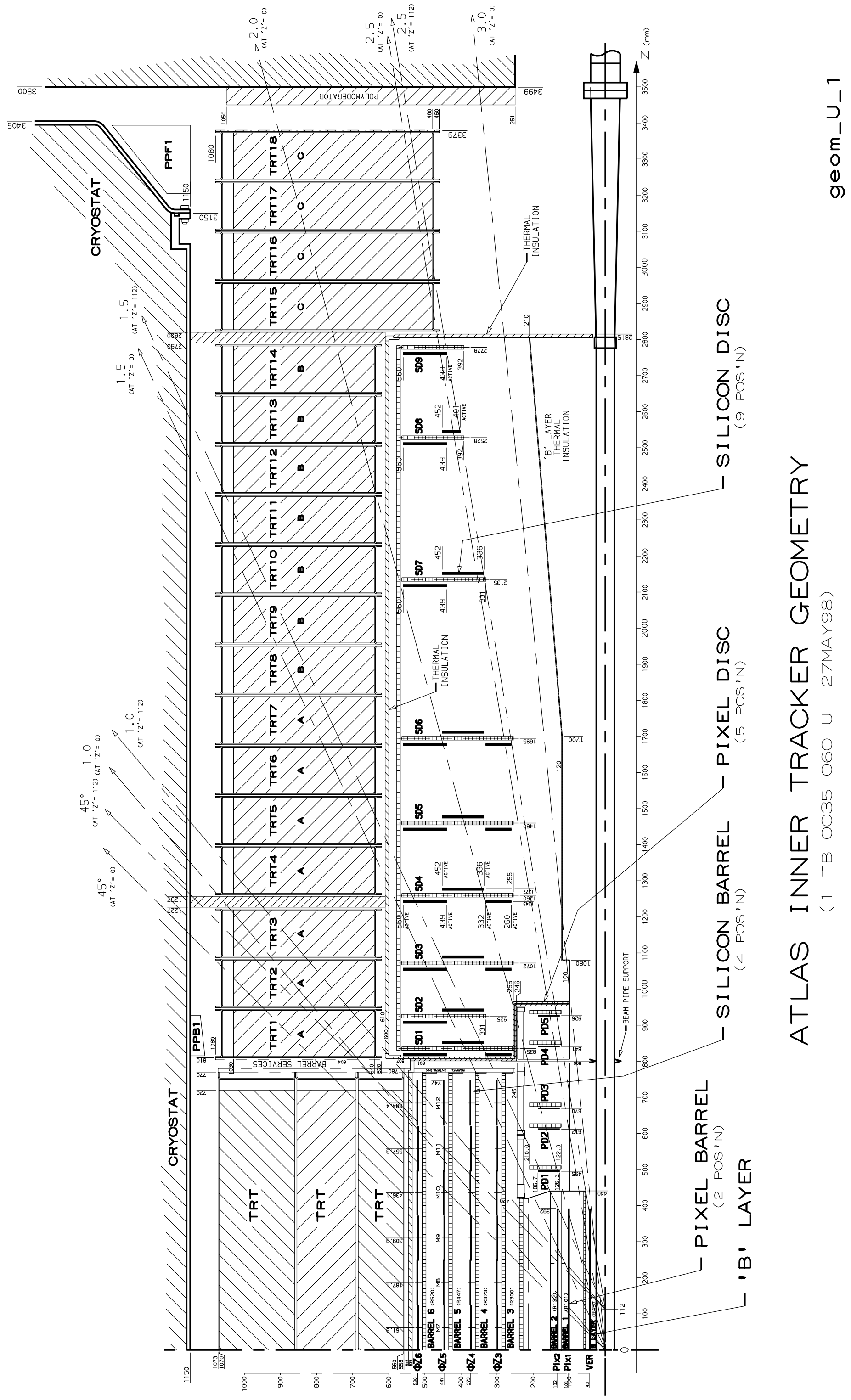

Figure 3-2 Current layout of Inner Detector.

5 Mechanical review

As stated in the action plan on material, a preliminary review of the ID mechanical engineering design was held on the 10-13th of November 1997. Three external reviewers took part, including one from ESTEC with experience of satellite design. The review committee was explicitly asked to consider the question of material reduction in the structures. It concluded:

“ *The ratio STRUCTURES/SERVICES (100kg/600kg) of the ID is quite comparable to the one commonly achieved for telecommunication satellites. The further optimisation of this ratio is deemed technically difficult and will certainly imply a significant increase in terms of both development risks and costs.*”

The review committee also commented on the difficulties of evaluating the stability of complex structures such as space frames, noting that FEA studies alone are not sufficient to give confidence in such designs, and that nodes and joints are likely to give stability problems. They recommended consideration of cylindrical shells instead. The design of the end-cap SCT support is therefore being reconsidered. The tradeoff depends on the level of access required through the structure to allow passage of services and for assembly tooling. Preliminary indications are that for the end-cap SCT geometry, there will be little difference in material if the spaceframe is replaced by a cylindrical support. This is an attractive option from the engineering point of view since it avoids the difficulties with nodes and joints noted by the committee, and gives a more uniform structure.

The comments made by the review committee on the need to prototype structures rather than relying on FEA calculations are also pertinent. The TRT designs have evolved over a number of years, with careful prototyping of full scale structures for barrel and end-cap at each stage. The TRT structures are especially critical because they support the precision detectors inside of them, and services running out of the ID volume. Overall the support mass is less than 1 g per straw in these prototypes, and the quality of the design work is shown by the fact that the only change which has been required since the ID TDR is to increase the thickness of the inner ring of the TRT end-cap wheels from the 1mm indicated by FEA to 2mm, a change of only 0.3% X_0, in order to meet the criteria of long-term straw stability and reliability of assembly procedures. This is included in the TRT plots below.

The review committee made a number of suggestions with respect to the services and their layout, intended to lead to an improved design. However, these recommendations are largely focussed on improvements to the practicalities of detector construction, installation and access, and in several cases would lead to increases in the material budget by adding extra connectors. The ID team is attempting on the contrary to resolve these practical issues without material increases, at the expense of a more difficult construction and operation scenario.

An example of this is the mounting of the modules on the SCT barrel. The original design called for a “local support” which would link modules together allowing a common test before mounting on the barrel. The solution now adopted uses direct mounting of each module directly onto the cylinder, improving the material by about 0.17% X_0 per layer, but giving a more difficult assembly and test procedure (see Section 7 for further details).

The ID audit of material has also considered several other options for futher optimisation of the material structure. Reducing the honeycomb fill thickness for the less heavily loaded parts of the SCT structures was considered but rejected on the grounds of practicality during manufacture. Consideration is being given to reducing the end-ring strength for smaller cylinders, but this will require further R&D. The replacement of the current CFRP skins on some support shells (thickness 200 microns, giving 350 g/m^2) by a Triax skin of 250-280 g/m^2 has also been discussed, but is not yet a feasible industrial option.

6 TRT

Even though the impact of material at small radius on the performance is considered to be largest [11-3], particular care has been put into minimising the amount of material in the TRT detector, as described in the engineering part of the Inner Detector Technical Design Report [11-2] and as shown in Figure 6-1.

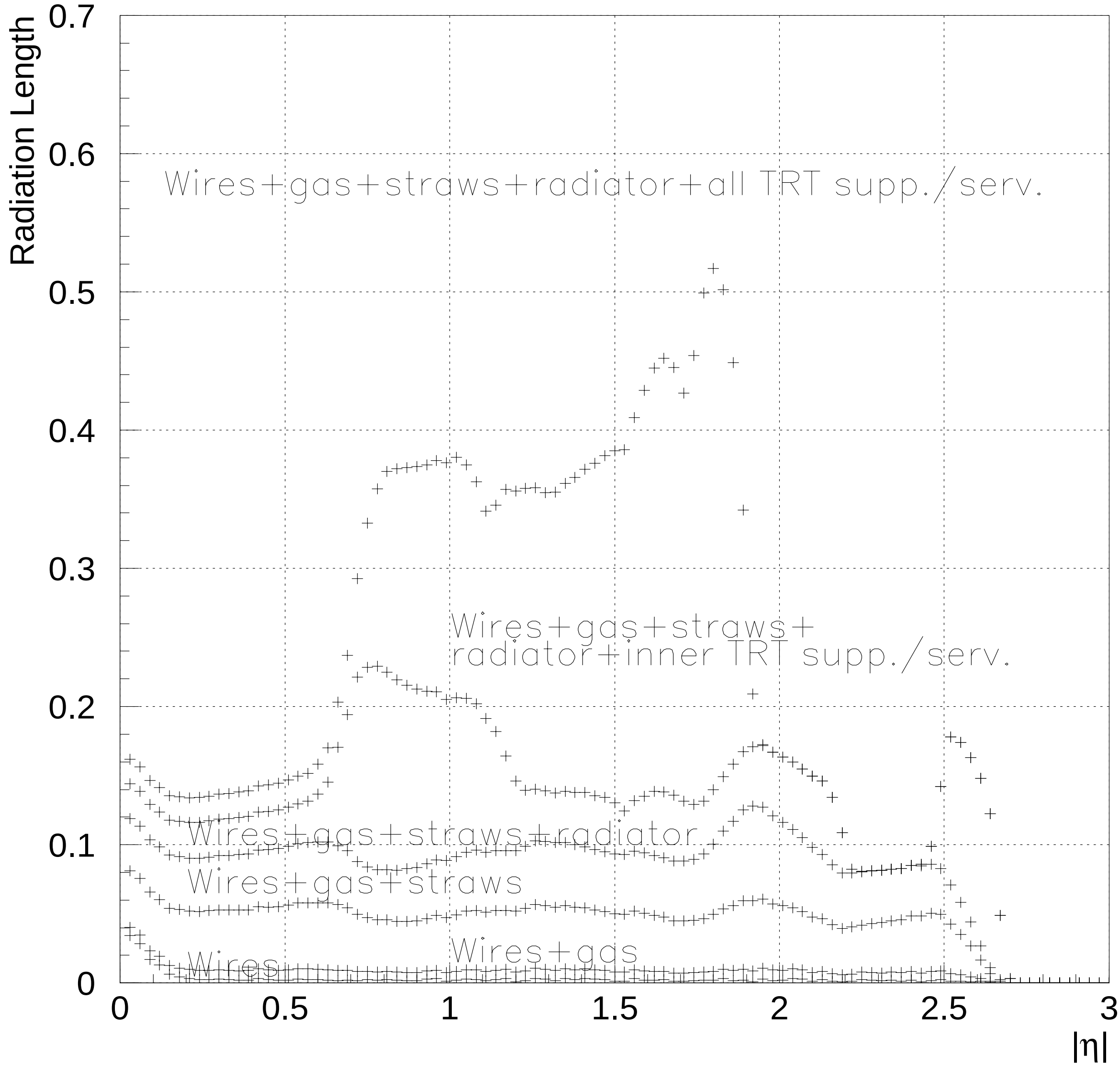

Figure 6-1 Cumulative distribution of TRT material (as presented in the TDR engineering estimates [11-2]) as a function of |η| (longitudinal vertex spread included).

Light-weight composite structures have been chosen for the mechanical support frames and the amount of metal has been kept at a minimum everywhere. In addition, the density of active detector elements (wires, gas, straws and radiator) has been chosen carefully, so as to maintain the total amount of active detector material to approximately 10% X_0 over the complete η-range. The abrupt increase of about 10% X_0 around η = 0.7 arises from the end-flange and services of the barrel TRT, and the significant additional increase at larger values of |η|, culminating at |η| = 1.8, is concentrated at the outermost radius of the tracker volume and arises from the outer enclosure of the TRT end-cap wheels and, to a lesser extent from the accumulation of all TRT services (barrel and end-cap).

Figure 6-2 shows in the same way as for Figure 6-1, the cumulative distribution of the TRT material, but as obtained from the best present engineering estimates. Considerable work has been undertaken since the

Inner Detector TDR to finalise the engineering design, in particular in terms of integration of services and electronics. This has resulted unavoidably in some increase of material at the outer radius. In the more sensitive part of the active volume, however, the changes are small, as described below.

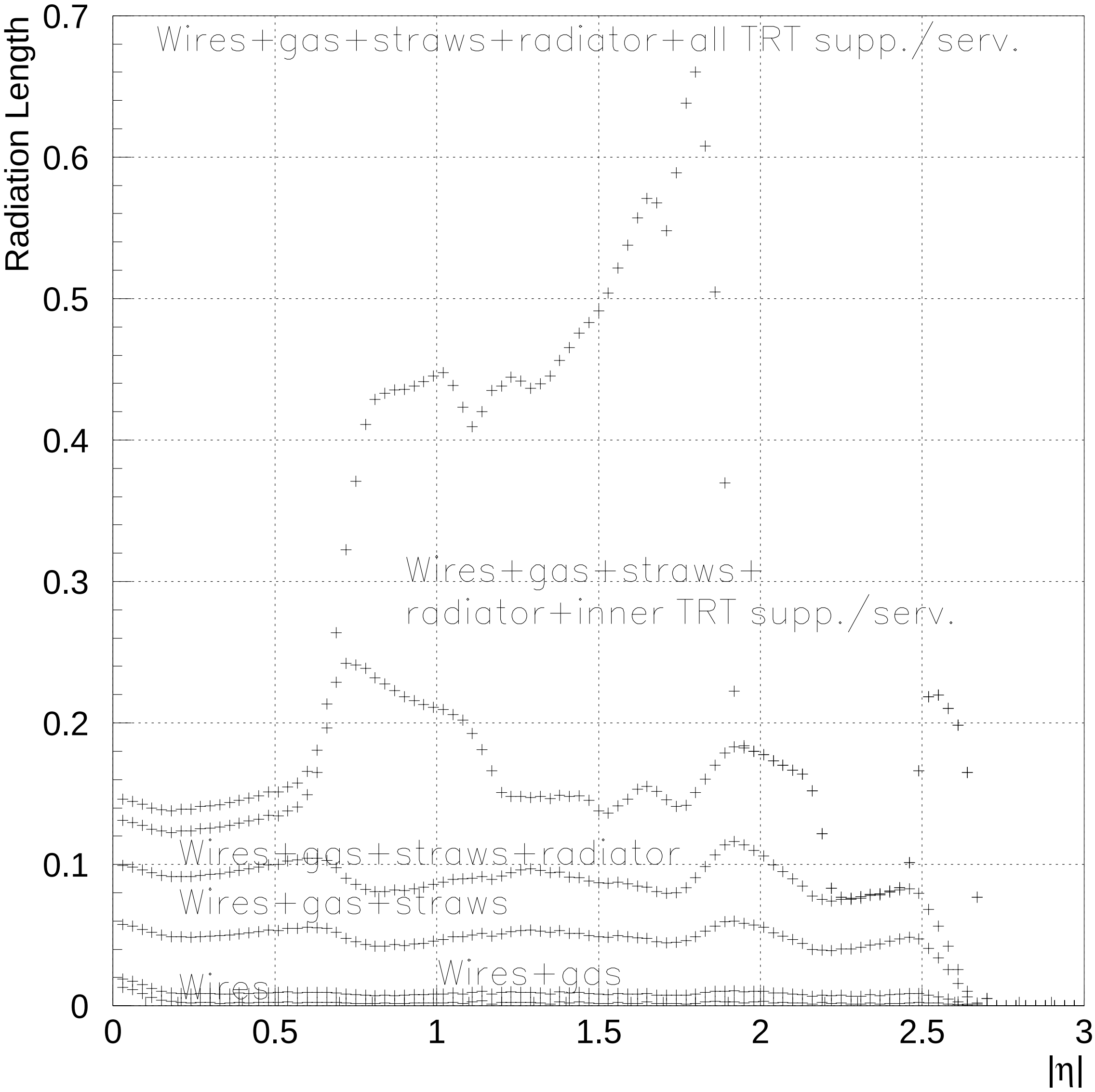

Figure 6-2 Cumulative distribution of TRT material (as obtained from best present engineering estimates) as a function of |η| (longitudinal vertex spread included).

6.1 Description of TRT material changes

The TRT detector is presently in its final stages of engineering design and pre-production modules are (or will be very soon) under construction both for the barrel and the end-cap. In addition to the more global issues of integration, connectivity and validation through experimental measurements and system tests, considerable effort has been put into possible reductions of the material in the sensitive area and into minimising the increases due to items not yet foreseen at the time of the TDR. Table 6-1 shows the best present engineering estimates put into the detector description and based most often on existing components and prototypes. The values are displayed as percentages of a radiation length for six characteristic η-bins (of width 0.03) and are averaged over the spread of the longitudinal vertex. The left-hand numbers

Table 6-1 Breakdown of the TRT material budget as a function of |η| (longitudinal vertex spread included). The left-hand numbers shown for each value of |η| represent the present best engineering estimate of the relevant material item, whereas the right-hand numbers represent the increase (or decrease) with respect to the numbers shown in the TDR.

	Radiation lengths in % X_0											
Pseudorapidity η	**0.0**		**0.6**		**0.9**		**1.2**		**1.78**		**2.2**	
Wires	1.3	*-2.1*	0.2	*0*	0.2	*-0.1*	0.3	*+0.1*	0.3	*0*	0.1	*-0.1*
Gas	0.6	*0*	0.7	*0*	0.6	*0*	0.7	*0*	0.7	*0*	0.6	*0*
Straw walls	3.9	*-0.1*	4.6	*-0.3*	3.6	*-0.1*	4.3	*-0.1*	4.3	*+0.1*	3.5	*-0.2*
Radiator	4.2	*+0.4*	4.9	*+0.5*	3.9	*-0.1*	4.2	*-0.3*	4.6	*-0.9*	3.5	*-0.3*
Barrel shells/cyl.	3.2	*+0.2*	3.5	*+0.3*	2.4	*+0.1*	0.1	*+0.1*				
Barrel end-flange and services			2.4	*+0.6*	10.7	*+0.5*	0.6	*-0.1*				
Inner end-cap enclosure							4.7	*+1.4*	5.8	*+1.8*		
Total: active volume	**13.1**	***-1.6***	**16.5**	***+1.2***	**21.6**	***+0.5***	**14.8**	***+1.1***	**16.0**	***+1.1***	**7.7**	***-0.5***
Outer end-cap enclosure					16.8	*+2.3*	20.8	*+2.7*	33.3	*+3.8*		
Outer services (barrel and end-cap)	1.5	*0*	1.6	*-0.1*	5.4	*+3.5*	8.9	*+4.9*	11.5	*+5.8*		
Total: outer volume	**1.5**	*0*	**1.6**	***-0.1***	**22.2**	***+5.8***	**29.7**	***+7.6***	**44.7**	***+9.5***		
Total: whole TRT	**14.6**	*-1.6*	**18.1**	***+1.1***	**43.8**	***+6.3***	**44.5**	***+8.7***	**60.8**	***+10.6***	**7.7**	***-0.5***
Uncertainty	±1.0		±1.0		±3.0		±3.0		±5.0		±1.0	

in each column represent the amount of material estimated for a given item and the right-hand numbers represent the increase (or decrease) with respect to the estimates shown in the TDR. Table 6-1 also shows two sub-totals for the TRT material, one for the so-called active volume which covers radii between 56 cm and 107 cm in the barrel and between 62 cm and 103 cm in the end-cap, the other for the so-called outer volume, which covers radii between the outer radius of the active volume and the position of the LAr barrel cryostat (radius of 115 cm). The uncertainties quoted in Table 6-1 correspond to the overall sum of the remaining uncertainties linked to final design and validation of certain technical solutions.

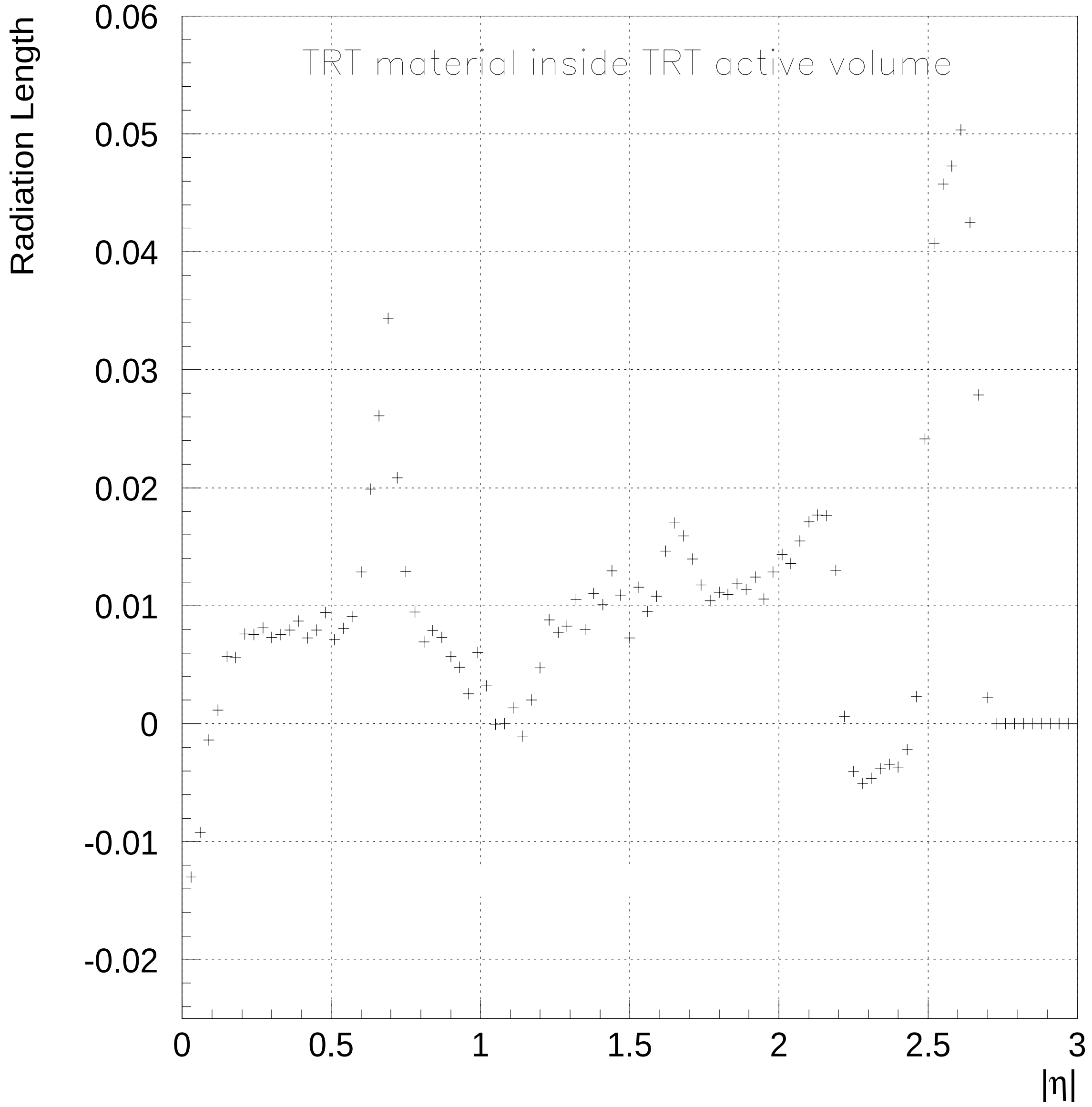

Figure 6-3 Distribution of the difference as a function of |η| (longitudinal vertex spread included) between the best present engineering estimates of the TRT material within the TRT active volume and those presented in the Inner Detector TDR.

As can be clearly seen from these sub-totals, the total material in the active volume has not changed much in either direction. This is better quantified in Figure 6-3, which shows the distribution of the increase (or decrease) of the TRT material in the TRT active volume as a function of |η| (see below for more details). On the other hand, the total material outside the TRT active volume, which is basically very close to the LAr barrel cryostat wall, has significantly increased, which is perhaps not surprising since this is the region where all the Inner Detector services have to be collected together, supported, and, specifically in the case of the TRT, connected to the end-cap wheels. As described below, this increase is due, in part to supports for services and connectivity details, which had not been included in the TDR, and in part to the more detailed and precise understanding of the layout of the outer enclosure of the TRT end-cap wheels. As illustrated more quantitatively in Figure 6-4, the maximum increase is almost 10% X_0 at $|\eta| \approx 1.8$.

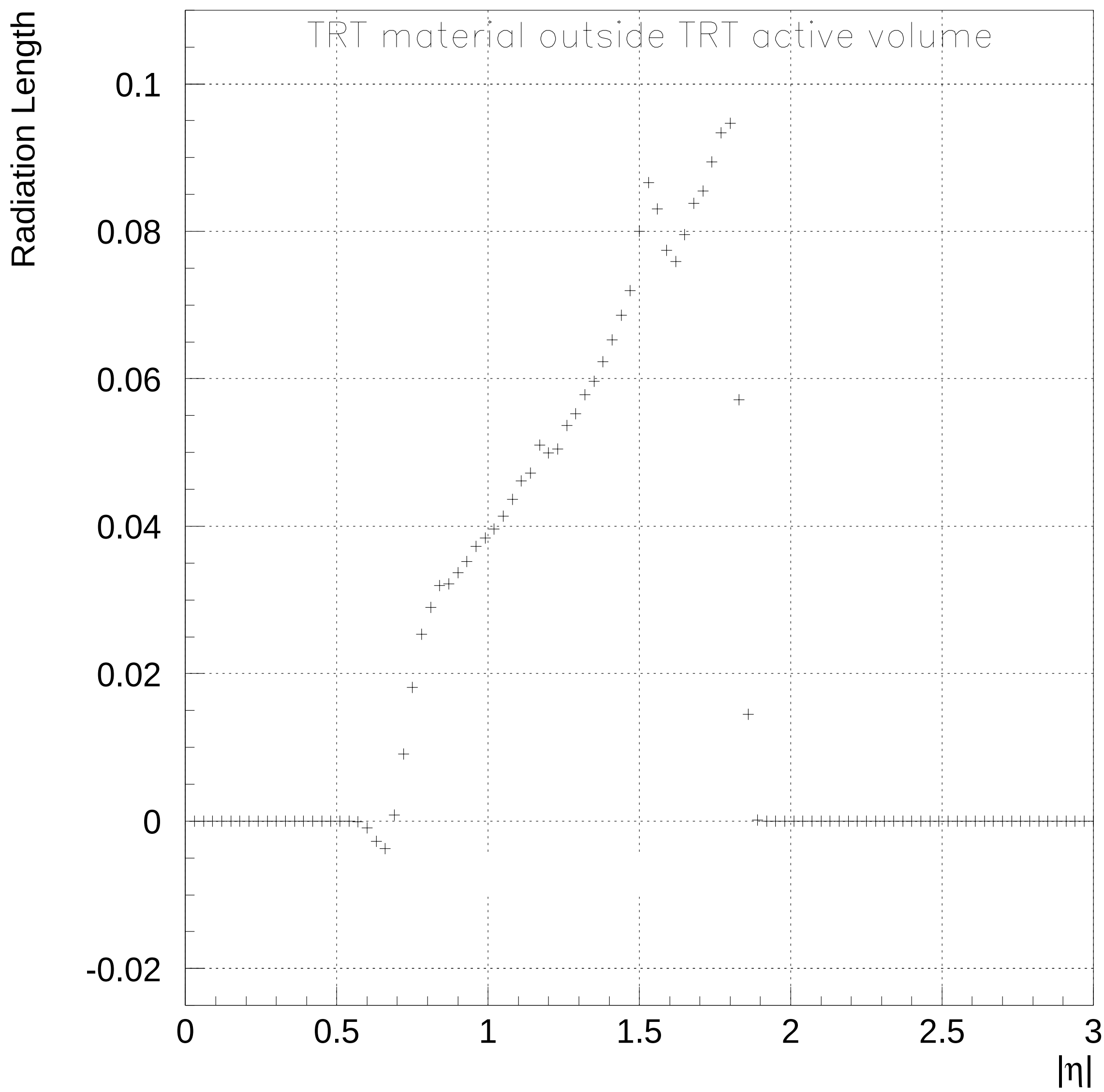

Figure 6-4 Distribution of the difference as a function of |η| (longitudinal vertex spread included) between the best present engineering estimates of the TRT material outside the TRT active volume and those presented in the Inner Detector TDR.

6.1.1 Changes within TRT active volume

The material within the TRT active volume can be divided into different functional categories, as illustrated in Figures 6-1 and 6-2 and described quantitatively in Table 6-1:

- the 30 μm diameter gold-plated tungsten wire, which amounts to a very small fraction of the total material of the active detector. However, in the barrel TRT, the wires are split in two in the middle and read out at both ends in order to reduce the single-channel occupancy. The wire-joints and wire-supports (twisters) used to achieve this appear as an average increase of 1.1% X_0 in the amount of material at $\eta = 0$ (the longitudinal vertex spread was included in the calculation of this increase). Thanks to a new and more aggressive design of these parts, a significant reduction of this contribution to the material (approximately a factor of 3) has been obtained (see Table 6-1);

- the ionisation gas (unchanged);
- the straws with their carbon-fibre reinforcement (essentially unchanged);
- the radiator (punched fibre mats in the barrel and thin foils in the end-cap). The amount of material due to the barrel radiator has slightly increased, since the diameter of the punched holes has been decreased from 5.2 mm to 4.8 mm to improve the electron identification performance, which is marginal at high luminosity in the barrel TRT. The amount of material due to the end-cap radiator has in contrast slightly decreased (the calculation is now based on existing polyproylene-foil industrially-produced radiator stacks);
- the carbon-fibre shells which define the barrel TRT modules (unchanged in design but described more accurately at present in the simulation);
- the barrel end-flanges and services, which include all the components used to fix and position the straws and wires mechanically and to connect them electrically, the electronics (chips, boards, connectors, etc) and the cables and fluid pipes. The breakdown of these different components is presented in Table 6-2 and compared to the corresponding estimates at the time of the TDR. It should be noted that the length of the barrel straws has not yet been frozen, since it depends on the exact length of the SCT barrel detector. The length used for the estimates presented here is slightly shorter than the one used for the TDR and the effect of this change in length can be seen in Figure 6-3 in the region $0.6 < |\eta| < 1.2$. Two full-length barrel modules have been manufactured and tested in

Table 6-2 Breakdown of the material budget for the end-flanges and services of the barrel TRT. The left-hand numbers represent the present best engineering estimate of the relevant material item, whereas the right-hand numbers represent the increase (or decrease) with respect to the numbers shown in the TDR. The numbers are computed at normal incidence, i.e. at a fixed average radius of about 80 cm.

Material (per side)	Radiation length in % X_0	
Straw-fixation plate	0.94	*+0.22*
Gas	0.02	*-0.03*
Straw end-plugs	0.38	*+0.10*
Straw-fixation elements	0.27	*0*
Blocking capacitors	0.32	*-0.19*
Wire-connection plate (tension plate)	0.90	*-0.05*
Wire-fixation elements	0.76	*-0.43*
Electronics boards and connectors	2.13	*-0.28*
Fuses and local HV connectors [a]	0.17	*+0.17*
Barrel support structure (space frame)	0.55	*+0.14*
Services: cables, fluids, pipes, fittings, cooling hardware	1.37	*+0.27*
Manifolds (Al pipes + fluorinert liquid) [b]	0.16 + 0.18 = 0.34	*+0.34*
Total	**8.15**	***+0.26***
Uncertainty	±2.0	

a. Not accounted for in the TDR (see text)

b. Not accounted for in the TDR (see text) beam since the TDR, and the design of the barrel modules is close to being finalised. As can be seen from Table 6-2, several of the components of the barrel end-flange have undergone significant reductions in material, but the net effect of the design progress since the TDR is nevertheless a small increase of 0.26% X_0, due mostly to engineering details in the area of cooling and of electrical services. The numbers in Table 6-2 still depend on certain assumptions about the final technical solutions which will be implemented once the barrel design is complete (this includes the front-end electronics and the barrel support structure). In particular, possible significant changes in the future could be:

a. an increase of the material due to electronics boards and connectors by 1.2% X_0, if a two-chip front-end electronics design has to be implemented rather than the preferred single-chip design;

b. an increase of the material due to the barrel support structure by 1.1% X_0, if the deformations under load of a full-size prototype structure turn out to be significantly larger than foreseen by the present calculations (it should be noted here that the specifications for the deformation under load of the barrel support structure are defined by the barrel SCT and the pixel detectors);

c. a decrease of the material due to the straw-fixation and tension plates by 0.6% X_0, if the overall mechanical design of the barrel TRT and the assembly procedures are shown to be compatible with plates of only 1 mm thickness.

For all the above reasons, the uncertainty shown in Table 6-2 for the amount of material due to the barrel end-flange and services is still quoted to be around ±2% X_0;

- the inner end-cap enclosure, situated at a radius of 62 to 64 cm for the type-A and type-B wheels and of 46 to 48 cm for the type-C wheels. The breakdown of the material budget for this enclosure is shown in Table 6-3. This enclosure was foreseen to be based on a 1 mm thick C-fibre ring at the

Table 6-3 Breakdown of the material budget for the inner enclosure of the end-cap TRT. The left-hand numbers shown for each wheel type represent the present best engineering estimate of the relevant material item, whereas the right-hand numbers represent the increase (or decrease) with respect to the numbers shown in the TDR. The numbers are computed at normal incidence, i.e. at a fixed z for each wheel type.

	Radiation length in % X_0					
Wheel type	**A**		**B**		**C**	
Carbon fibre support ring (2 mm thick)	0.62	*+0.31*	0.68	*+0.34*	0.62	*+0.31*
Aluminised polyimide cover	0.30	*+0.04*	0.30	*+0.04*	0.30	*+0.04*
Gas (about 1.5 cm thick)	0.11	*+0.02*	0.11	*+0.02*	0.11	*+0.02*
Wire crimping pins	0.80	*+0.21*	0.40	*+0.11*	0.80	*+0.21*
Straw fixation rings	0.10	*0*	0.05	*0*	0.10	*0*
Straw end-plugs and moulded pieces	0.68	*+0.17*	0.34	*+0.08*	0.68	*+0.17*
Total [a]	**2.62**	***+0.76***	**1.89**	***+0.60***	**2.62**	***+0.76***
Uncertainty	±0.5		±0.5		±0.5	

a. Cooling gas manifolds (three in total per side) have not been included here time of the TDR, but this thickness has been increased to 2 mm after a careful evaluation of the assembly steps and tooling required to implement a tension per straw sufficient to make sure that no straw is ever under compression once the detector is in place. This decision has been recently validated by prototyping of the precise tooling required for its implementation in the assembly of the first pre-production module. Given its position at the innermost radius of the end-cap TRT, this inner enclosure has been designed to be as lightweight as compatible with a safe mechanical design (thickness of carbon-fibre support ring, dimensions of plastic elements and, more importantly, of metallic crimping pins). As shown in Table 6-3, the final design values for several of these elements are higher than those of the TDR because of the conflicting engineering requirements for a robust and reproducible assembly procedure. It should be noted here that the total mass of the end-cap mechanical support structures can be expressed as approximately 1 g per straw (these CFRP structures are drilled with many thousands of precision holes).

6.1.2 Changes outside TRT active volume

The material outside the TRT active volume can be divided into two different functional categories, as summarised in Table 6-1 and described in more detail below (see also Tables 6-4 and 6-5):

Table 6-4 Breakdown of the material budget for the outer enclosure of the end-cap TRT. The left-hand numbers shown for each wheel type represent the present best engineering estimate of the relevant material item, whereas the right-hand numbers represent the increase (or decrease) with respect to the numbers shown in the TDR. The numbers are computed at normal incidence, i.e. at a fixed z for each wheel type.

	Radiation length in % X_0					
Wheel type	**A**		**B**		**C**	
Inner carbon support ring (4 mm thick)	1.08	*0*	1.28	*0*	1.18	*0*
Straw end-plugs and moulded pieces	1.16	*-0.02*	0.58	*-0.01*	0.86	*-0.03*
Gas	0.11	*-0.02*	0.11	*-0.03*	0.11	*-0.02*
Crimping pins	2.11	*+1.60*	1.06	*+0.81*	1.59	*+1.21*
Outer carbon support ring (4 mm thick)	1.34	*0*	1.41	*0*	1.37	*0*
Wire and HV connection board (active WEB)	1.86	*0*	1.45	*0*	1.65	*0*
Passive connection flange (passive WEB)	0.68	*0*	0.68	*0*	0.68	*0*
Fluid pipes (containing fluorinert liquid [a])	0.73	*+0.07*	0.73	*+0.07*	0.73	*+0.07*
Electronics boards and connectors	2.80	*0*	2.46	*0*	2.63	*0*
Total [b]	**11.87**	***+1.63***	**9.76**	***+0.84***	**10.80**	***+1.23***
Uncertainty	±1.5		±1.5		±1.5	

a. The corresponding values for the TDR were computed for water as coolant

b. Fittings for the gas and liquid cooling pipes and possible heat exchangers have not been included (see text)

- the outer end-cap enclosure (situated at a radius of 103 to 108 cm for all wheels), which, similarly to the barrel end-flange, comprises all components necessary to position and fix the straws and wires mechanically, the electronics, and the services. The breakdown of the individual components is shown in Table 6-4. The only significant change with respect to the TDR is an increase of 0.8%

to 1.6% X_0 of the crimping pins which have been finally chosen as fully metallic rather than plastic/metal composites due to concerns about the long-term reliability of these crucial components for the wire fixation and the electrical signal connection. Table 6-4 does not explicitly include fittings for the gas and liquid cooling pipes (a small contribution since only a few pipes are foreseen per wheel), nor does it include the amount of material which might come from heat exchangers, which would have to be added (18 heat exchangers per side) if the present scheme for extracting the heat from the gas into the cooling liquid for the electronics were shown to be not viable;

- in order of increasing radius beyond the envelope of the outer end-cap enclosure (R = 108 cm):

  a. the so-called squirrel cage (designed such as to support both the TRT end-cap and SCT end-cap services, while permitting sufficient access to the TRT wheels to connect them to their respective cables and pipes). This squirrel cage had not yet been designed in any detail at the time of the Inner Detector TDR, and was not included explicitly in the material description at that time. As shown in Table 6-5, it amounts to a total of 1.55% X_0 of material (at normal incidence);

  b. cable trays for the end-cap services, which for the same reasons had not been included explicitly at the time of the Inner Detector TDR. They amount to a total of 0.52% X_0 of material (at normal incidence);

  c. end-cap fluid pipes and electrical services. These have increased significantly (by 1.39% X_0 at normal incidence), due mostly to a detailed layout of the low-voltage power distribution assuming conservatively a power of 60 mW per front-end channel and a maximum power dissipation in the low-voltage cables themselves of 1 kW within the Inner Detector volume. It should be noted that the TRT low-voltage power cables are assumed not to need any cooling in these conditions. A small increase due to the change of coolant from water to fluorinert has also been included in the numbers shown in Table 6-5;

Table 6-5 Breakdown of the material budget for the outer services of the TRT at two locations in z near the wall of the barrel LAr cryostat (R = 114 cm). The left-hand numbers shown for each location and computed at normal incidence (fixed z) represent the present best engineering estimate of the relevant material item, whereas the right-hand numbers represent the increase (or decrease) with respect to the numbers shown in the TDR.

	Radiation length in % X_0			
Position (radius of 114 cm)	*Barrel : z = 830 mm*		*End of end-cap : z = 3300 mm*	
Squirrel cage (Aluminium) [a]	0	*0*	1.55	*+1.55*
Cable trays [b] (plastic 2 mm thick)	0.20	*+0.20*	0.52	*+0.52*
Fluid/gas services [c]	0.43	*+0.03*	0.85	*+0.07*
Electrical services	0.96	*+0.58*	4.00	*+1.93*
(Electrical services with LV in Al)	(0.47)	*(+0.09)*	(2.08)	*(0)*
Total (with LV in Al) [d]	**1.59 (*1.10*)**	***+0.81 (+0.32)***	**6.92 *(5.00)***	***+4.07 (+2.15)***

a. Not accounted for in the TDR

b. Not accounted for in the TDR

c. Cooling fluid is assumed to be fluorinert

d. Total assumes copper is used for low-voltage power cables, i.e. sum excludes fifth row. Numbers in brackets assume Aluminium is used for low-voltage power cables i.e. sum excludes fourth row (see text)

d. barrel fluid-pipes and electrical services. These have increased by 0.61% X_0 at normal incidence for the same reasons as described above for the end-cap services.

The overall increase in this region at large radius, which is still under intensive engineering study (patch-panels, installation/maintenance scenario, etc.) as discussed in Section 9, peaks around 10% X_0. as illustrated in Figure 6-4. The impact of this increase on the Inner Detector and calorimeter performances is very small (see Section 10).

Nevertheless, in an attempt to further minimise the overall amount of material in services, the possible use of aluminium cables for the low-voltage power is under study for the TRT. As shown in Table 6-5, the amount of material due to electrical services would be reduced by approximately a factor 2, from 4% X_0 to 2% X_0, if such a technical option could be adopted. Potential serious disadvantages of the aluminium option are the extra space required for the services for the same power dissipation (the total cross-sectional area required for all TRT services at the exit of the Inner Detector volume would increase from 850 cm^2 to 1000 cm^2), the cost of cables fully equipped with connectors, and technical aspects related to the higher rigidity of aluminium with respect to copper and the risks of corrosion for direct aluminium-to-coper/brass connections.

7 SCT

The detailed changes to the SCT material since the TDR engineering design are given in Table 7-1 and Table 7-2, below, which follow the format of those in the TDR for convenience. The main differences are:

- changes to the barrel material due to the removal of local supports in favour of direct mounting of the modules onto the support cylinders (reduction of 0.17% X_0 per layer);
- changes to the cooling pipes assuming that the evaporative system is adopted. This decision has still to be taken, together with the final choice of pipe modularity (see Section 4);
- small changes in the material of the end-cap spaceframe, which is now a single unit, due to the adoption of 10mm rather than 8mm pipes (required to meet the stiffness criteria following more detailed FEA studies) and an improved estimate of the joint thickness. For comparison with the TDR, four entries have been retained in the tables. The alternative of a cylindrical support shell is being considered (see Section 5);
- an improved description of the thicknesses of end-cap modules which vary from ring to ring. These have been averaged over the whole disk to facilitate comparison with the TDR;
- the end-cap wheel value is now for the bare carbon fibre disk, and the end-cap cabling services now include the cooling pipes, coolant, 4 types of cooling block, 2 types of end-tab block, fasteners, power cables and fibre optics. Connectors at the outer rim of the disks may be needed in order to make access and maintenance simpler: these are not included;
- the barrel patch panel estimate has been reduced: the number given here now corresponds to a separate panel for SCT alone, rather than a combined panel with the pixels as foreseen in the TDR. Part of the reduction is therefore artificial, with the corresponding material included in the pixel tables. However, part of the reduction is due to real improvements in the materials used (see Section 9);
- the end-cap power tapes will require independent cooling circuits which have not yet been designed. The estimated thickness will be 0.15% X_0 in the cylindrical region and 0.25% X_0 in the planar region. These values have been included;

Table 7-1 Comparison of the material in the SCT in cylindrical form for the ID TDR and the present designs.

Item	Mean R (mm)	Z min. (mm)	Z max. (mm)	% X_0 in ID TDR	% X_0 now
Barrel 3 carbon fibre cylinder	275	0	790	0.265	0.265
Barrel 3 module mountings,cooling	285	0	790	0.386	0.227
Barrel 3 modules	300	0	790	1.298	1.246
Barrel 3 power tapes	285	0	790	0.130	0.130
Barrel 3 power connectors	285	0	790	0.070	0.070
Barrel 3 opto hybrids and fibres	285	0	790	0.023	0.023
Barrel 3 cooling manifold	290	769	790	1.380	1.380
Barrel 4 carbon fibre cylinder	349	0	790	0.265	0.265
Barrel 4 module mountings,cooling	359	0	790	0.386	0.227
Barrel 4 modules	373	0	790	1.306	1.298
Barrel 4 power tapes	359	0	790	0.130	0.130
Barrel 4 power connectors	359	0	790	0.070	0.070
Barrel 4 opto hybrids and fibres	359	0	790	0.023	0.023
Barrel 4 cooling manifold	364	769	790	1.640	1.640
Barrel 5 carbon fibre cylinder	422	0	790	0.265	0.265
Barrel 5 module mountings,cooling	432	0	790	0.386	0.227
Barrel 5 modules	447	0	790	1.309	1.300
Barrel 5 power tapes	432	0	790	0.130	0.130
Barrel 5 power connectors	432	0	790	0.070	0.070
Barrel 5 opto hybrids and fibres	432	0	790	0.023	0.023
Barrel 5 cooling manifold	438	769	790	2.220	2.220
Barrel 6 carbon fibre cylinder	495	0	790	0.305	0.265
Barrel 6 module mountings, cooling	505	0	790	0.433	0.227
Barrel 6 modules	520	0	790	1.313	1.303
Barrel 6 power tapes	505	0	790	0.130	0.130
Barrel 6 power connectors	505	0	790	0.070	0.070
Barrel 6 opto hybrids and fibres	505	0	790	0.023	0.023
Barrel 6 cooling manifold	512	769	790	2.540	2.540
Barrel region active insulation	539	0	822	0.496	0.647
Barrel patch panel	1150	790	890	5.600	1.900
End-cap support structure, module	575	835	1178	0.309	0.310

Table 7-1 Comparison of the material in the SCT in cylindrical form for the ID TDR and the present designs.

End-cap support structure, module	575	1178	1589	0.268	0.310
End-cap support structure, module	575	1589	2343	0.273	0.310
End-cap support structure, module	575	2343	2830	0.294	0.310
End-cap services	600	830	925	0.177	0.135
End-cap services	600	925	1072	0.177	0.234
End-cap services	600	1072	1280	0.177	0.369
End-cap services	600	1280	1460	0.197	0.504
End-cap services	600	1460	1695	0.197	0.639
End-cap services	600	1695	2135	0.197	0.774
End-cap services	600	2135	2528	0.197	0.874
End-cap services	600	2528	2778	0.197	0.975
End-cap services	600	2778	2800	0.197	1.042
End-cap region active cooling	610	822	2825	0.496	0.637
End-cap cabling services	1150	2810	3405	0.360	0.560
End-cap cooling services	1150	2810	3405	1.176	0.151
Barrel cabling services	1150	815	3405	0.856	0.450
Barrel cooling services	1150	815	3405	0.976	0.420
End-cap patch panel	1150	3305	3405		2.500

- all end-cap services now exit between TRT wheels 14 and 15. The TDR numbers have been recomputed for the appropriate z slices for comparison.

Work has been proceeding on the prototyping of novel hybrid designs, using kapton or pyrolytic graphite. If these designs are adopted, a further saving of approximately 0.13% X_0 could be expected in the module thickness. This is not included in the tables.

The figure given for the active insulation corresponds to the existing design. There is still scope here for further trade-off between the total material and the temperature uniformity.

Small changes may also be expected in the opto-boards once the VCSEL design is finalised.

The total change in the SCT material between this design and layout 97-6 is shown in Figure 2-6. The material in the barrel region has been reduced, while that in the end-cap region has increased due to the re-routing of the services, compared to that simulation.

8 Pixels

The material in the pixel system has been re-evaluated in detail in the pixel TDR. This section reproduces the information presented there.

Table 7-2 Comparison of the material in the SCT in planar form for the ID TDR and present designs.

Item	Mean Z (mm)	R min. (mm)	R max. (mm)	% X_0 in ID TDR	% X_0 now
Barrel 3 carbon fibre cylinder end	780	255	280	0.9	0.9
Barrel 4 carbon fibre cylinder end	780	323	353	0.9	0.9
Barrel 5 carbon fibre cylinder end	780	387	427	0.9	0.9
Barrel 6 carbon fibre cylinder end	780	460	500	0.9	0.9
Interlinks	788	245	530	0.498	0.498
Barrel/end-cap insulation	780	240	546		0.108
Barrel/end-cap insulation	805	240	610		0.108
Barrel 3 cabling services	815	285	550	0.21	0.21
Barrel 3 cooling services	815	290	550	0.044	0.044
Barrel 4 cabling services	815	359	550	0.242	0.242
Barrel 4 cooling services	815	364	550	0.048	0.048
Barrel 5 cabling services	815	438	550	0.272	0.272
Barrel 5 cooling services	815	432	550	0.056	0.056
Barrel 6 cabling services	815	505	550	0.291	0.291
Barrel 6 cooling services	815	512	550	0.064	0.064
All barrels cabling services	815	550	1150	0.568	0.59
All barrels cooling services	815	550	1150	0.22	0.504
End-cap wheel 1	835	260	560	0.898	0.248
End-cap wheel 1 modules	835	260	560	1.529	1.359
End-cap wheel 1 cabling services	835	260	560	0.17	1.159
End-cap wheel 2	925	336	560	0.912	0.248
End-cap wheel 2 modules	925	336	560	1.402	1.259
End-cap wheel 2 cabling services	925	336	560	0.14	0.989
End-cap wheel 3	1072	260	560	0.898	0.248
End-cap wheel 3 modules	1072	260	560	1.529	1.359
End-cap wheel 3 cabling services	1072	260	560	0.17	1.159
End-cap wheel 4	1260	260	560	0.898	0.248
End-cap wheel 4 modules	1260	260	560	1.529	1.359
End-cap wheel 4 cabling services	1260	260	560	0.17	1.159
End-cap cabling services	1280	570	1150	0.288	0
End-cap cooling services	1280	570	1150	0.736	0

Table 7-2 Comparison of the material in the SCT in planar form for the ID TDR and present designs.

End-cap wheel 5	1460	260	560	0.898	0.248
End-cap wheel 5 modules	1460	260	560	1.529	1.359
End-cap wheel 5 cabling services	1460	260	560	0.17	1.159
End-cap wheel 6	1695	260	560	0.898	0.248
End-cap wheel 6 modules	1695	260	560	1.529	1.359
End-cap wheel 6 cabling services	1695	260	560	0.17	1.159
End-cap wheel 7	2135	336	560	0.912	0.248
End-cap wheel 7 modules	2135	336	560	1.402	1.259
End-cap wheel 7 cabling services	2135	336	560	0.14	0.989
End-cap wheel 8	2528	401	560	0.992	0.248
End-cap wheel 8 modules	2528	401	560	1.596	1.417
End-cap wheel 8 cabling services	2528	401	560	0.18	1.29
End-cap wheel 9	2776	401	560	0.833	0.248
End-cap wheel 9 modules	2776	401	560	1.397	1.25
End-cap wheel 9 cabling services	2776	401	560	0.15	0.956
End-cap cabling services	2810	570	1150	0.243	0.8
End-cap cooling services	2810	570	1150	0.752	0.113
Active cooling end plate	2825	30	585	0.532	0.623

The design of the pixel system has evolved substantially and is significantly more mature than at the time of the publication of the Inner Detector TDR in April 1997. The material in all aspects of the pixel system has been re-estimated. However, a number of different design options for modules and mechanics remain, and these are described in the pixel TDR. Some comparisons among these options are also summarised here.

8.1 Pixel Sub-System Material Distribution

The material distribution in radiation lengths as a function of rapidity is shown in Figure 8-1. This plot only includes material within the pixel system, i.e. within a radius of 25 cm.

8.2 Comparison with Previous Estimates of Pixel Material

A summary comparison of the average material in the pixel system in radiation lengths as estimated now and one year ago for the ID TDR (Vol. II) is given in Table 8-1. The material in the pixel services has decreased as a result of the adoption of evaporative cooling. A complete conceptual design for the pixel supporting structures now exists, and the estimates of the material in these structures has increased in the active volume in the last year. In addition, the need for a thermal barrier to allow removal of the B-layer

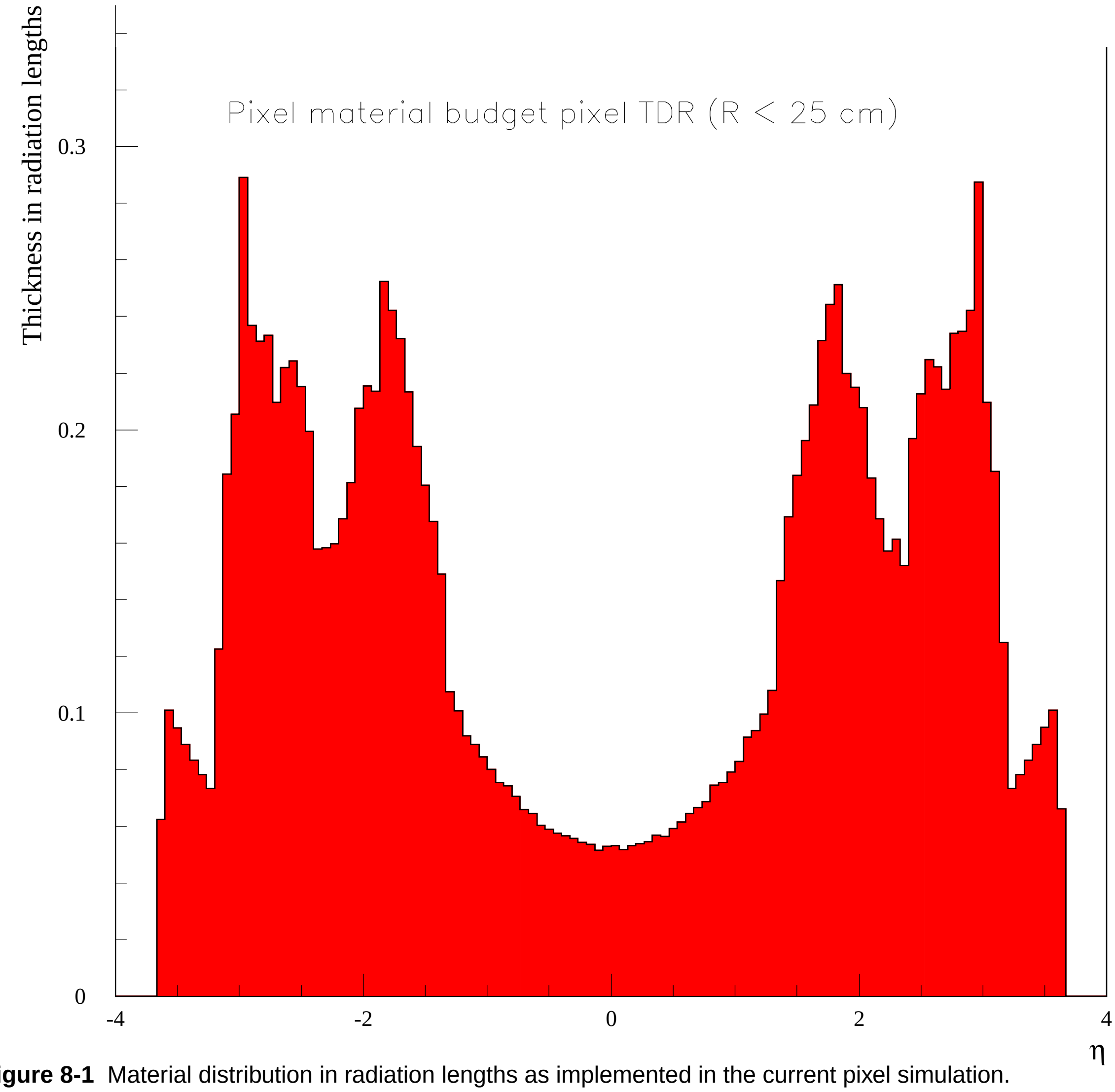

Figure 8-1 Material distribution in radiation lengths as implemented in the current pixel simulation.

Table 8-1 Summary comparison of average material in radiation lengths in the pixel system and related services as estimated now and at the time of the Inner Detector Technical Design Report.

Region	ID TDR $|\eta|<3.7$	Pixel TDR $|\eta|<3.7$	ID TDR $|\eta|<2.5$	Pixel TDR $|\eta|<2.5$
R<25 cm	13.8%	13.4%	11.2%	12.9%
R>25 cm	1.6%	1.0%	2.3%	1.3%
Total	15.4%	14.4%	13.5%	14.2%

and vacuum pipe bake-out has been included in the current estimates and was not present in the ID TDR. This barrier is a significant addition to the material, particularly in the end-cap region. The net effect is that the current estimate of the material in the active volume of the pixel system has increased somewhat since the publication of the ID TDR. A more detailed comparison of the different elements in the material estimate is given below.

Table 8-2 presents a summary comparison between the material at normal incidence in the barrel region. as currently estimated for one combination of module and stave mechanics design, and the estimates made at the time of the ID TDR. C_4F_{10} evaporative cooling is assumed in the current estimate, while binary ice cooling was assumed for the estimate in the ID TDR (assuming C_4F_{10} evaporative cooling for the designs described in the ID TDR would reduce the module/stave material by about 0.15%). The current material estimates shown in Table 8-2 are for the “stepped” (chips-down) stave with an aluminium-kapton power bus. The values shown for the barrel modules + staves vary because of slightly different overlap factors for the three different layers, and because the detectors are assumed to be 200 μm thick for the B-layer. The estimates shown do not include services and supports at the end of the barrel region.

Table 8-2 Material comparison in the barrel region (as explained in the text) between the pixel current design and that described in the Inner Detector Technical Design Report (Vol. II).

	Radiation Length (%X_0) Now	Radiation Length (%X_0) ID TDR
B-layer modules/staves	1.38	1.45-1.81
B-layer support shell	0.32	0.11
Inner thermal barrier	0.22	0
Layer 2 modules/staves	1.44	1.45-1.81
Layer 2 support shell	0.17	0.11
Layer 3 modules/staves	1.46	1.45-1.81
Layer 3 support shell	0.17	0.11
Outer system support	0.2	0.2

The estimated material in the modules + staves has remained within the window calculated at the time of the ID TDR. The material needed for supporting structures has increased. At that time, no design existed for the support structures, while now there is a nearly complete conceptual design. The need for beam-pipe bakeout and hence a thermal barrier between the B-layer and layers 2 and 3 has only recently been realised.

Prototype disk sectors have already been constructed with an average radiation length of about 0.75-0.85% X_0 (over the active region), and it may be possible to reduce this by about 0.15% X_0 if thinner face plates are feasible. Therefore it is expected to be possible to fabricate disk sectors with a radiation length in the range 0.60-0.85% X_0, compared with the expectation at the time of the ID TDR of 0.62-1.07% X_0. If aluminium-on-kapton hybrids are used for the disk module interconnections, the total average radiation length in the active region of the disk would be in the range of 0.60-0.85% (sector) + 0.80% (modules with overlap) = 1.40-1.65% X_0. The disk design presented in the ID TDR had interconnect hybrids outside the active region (at larger radius) that have been eliminated in the current design. In addition, the estimated material in the disk support rings has been reduced. The estimated material in the spaceframe that supports the disks has increased from 0.2% X_0 to 0.36% X_0. In addition, there are now thermal barriers (0.22% X_0) at the outer radius and on the ends of the disk system and these were not present at the time of the ID TDR.

It is more difficult to present an item-by-item comparison of the material in the services. Very crudely, the material in power cables has increased somewhat since the estimate made in the ID TDR and the material in the coolant pipes and coolant has decreased significantly by the adoption of C_4F_{10} evaporative cooling. The net effect of these changes is to somewhat reduce the total amount of material in the pixel services. This is most easily seen by comparing the material in the services outside the pixel volume as estimated now with a similar estimate at the time of the ID TDR (Figure 8-2).

Figure 8-3 compares the total material in supporting structures (including the thermal barrier), overall support structures and services within the pixel volume (r < 25 cm), as estimated now and at the time of

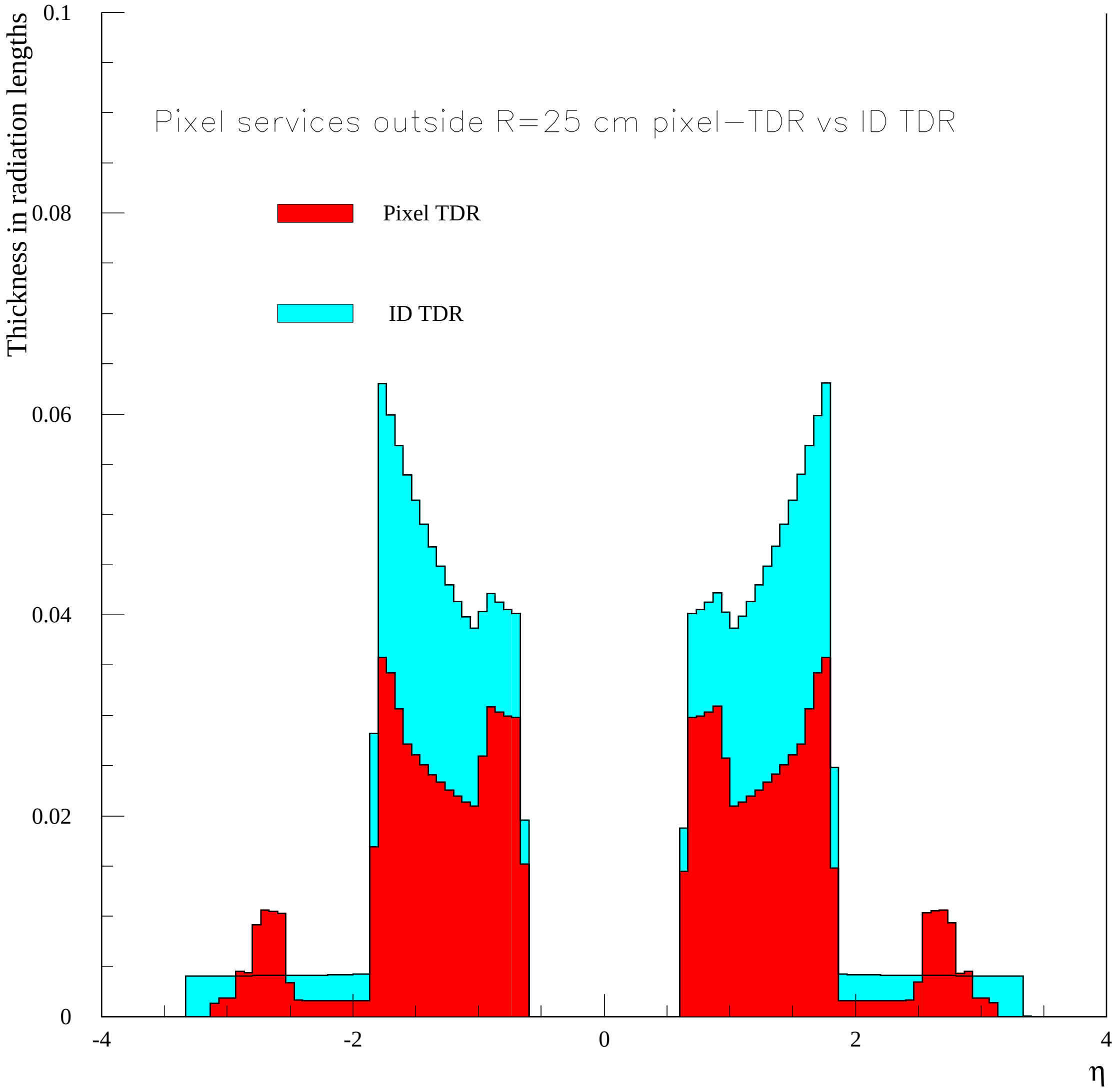

Figure 8-2 Estimate of material in pixel services(R>25 cm) now and at the time of the Inner Detector TDR.

the ID TDR. The increase in the material in the supporting structures, due particularly to the need for a thermal barrier, is somewhat greater than the decrease made in services. In Figure 8-4, the comparison is made between the detector services, but excluding the overall support structure and B-layer thermal barrier. It should be pointed out that the thickness of the B layer support shell is greater than that of the other barrel layers (Table 8-7), and greater than the value assumed in the ID TDR, since these have to be clam-shelled around the beam pipe with remote manipulators. Efforts will be made to reduce this contribution.

Figure 8-5 compares the total material ($r < 25$ cm) as estimated now, and as estimated at the time of the ID TDR (and implemented in the simulations comparing 6 vs 7 precision layers[11-3]). The difference in material is shown in Figure 8-6. Possibilities for further material reduction are presented at the end of this section.

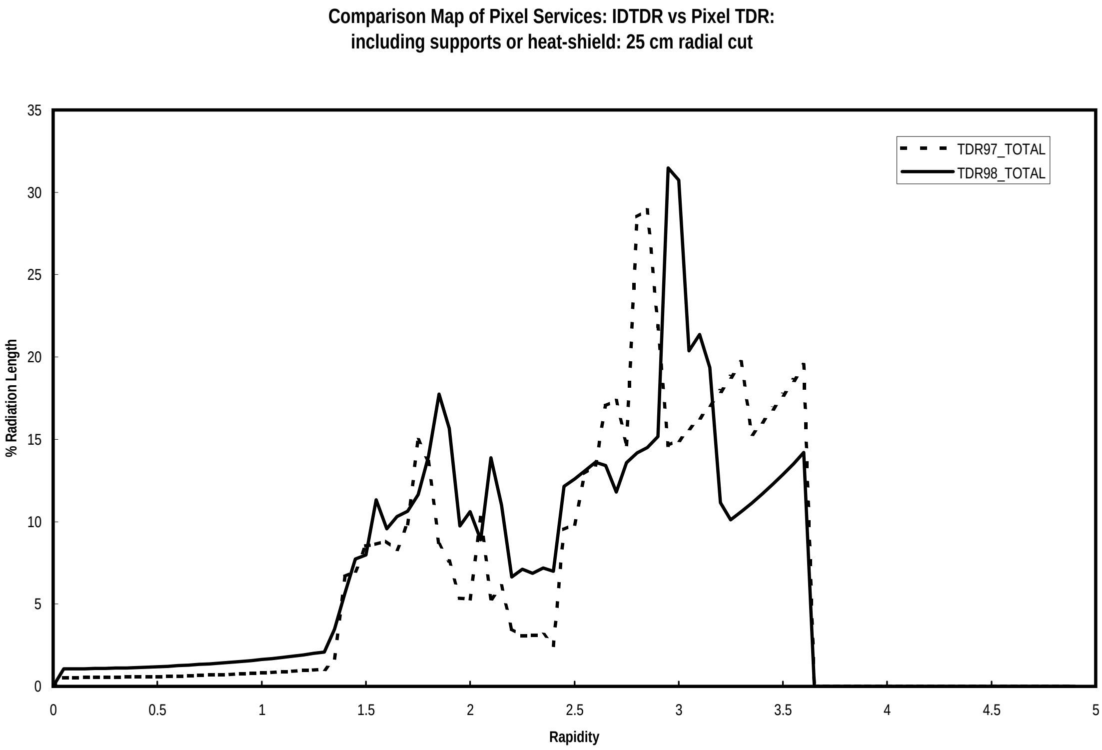

Figure 8-3 Comparison of Pixel Services and Supports in the pixel TDR with those of the ID TDR (April 30, 1997). In the pixel TDR, the B-layer thermal screen is included.

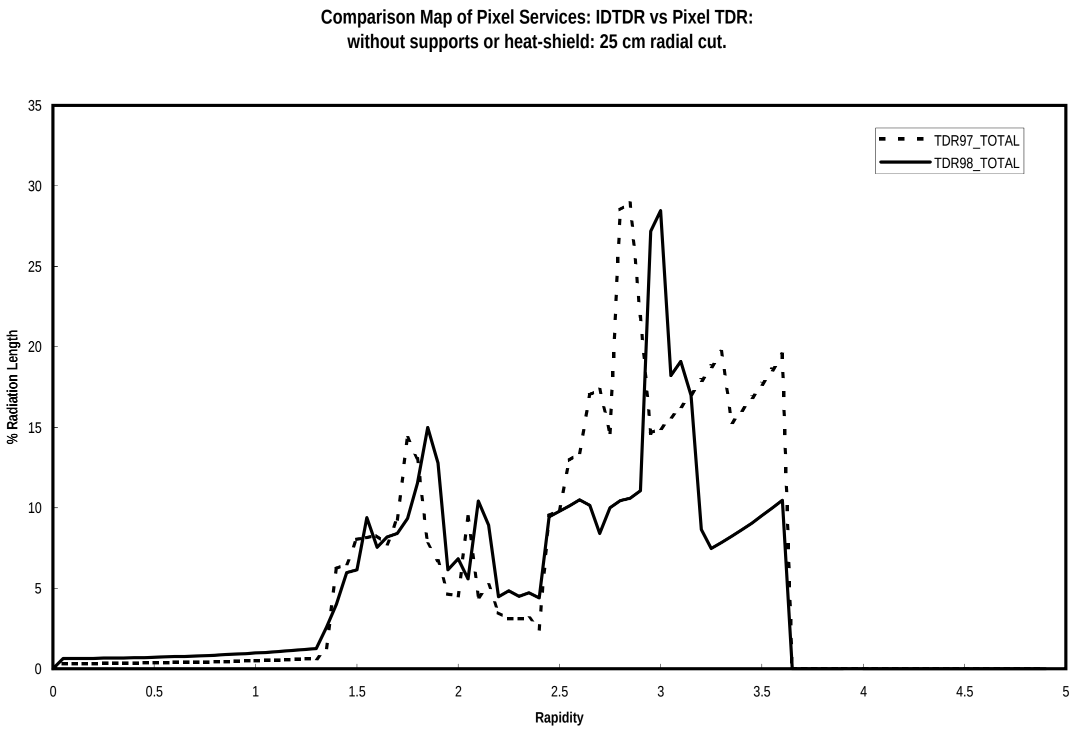

Figure 8-4 Comparison of Pixel Services and Supports in the pixel TDR with those of the ID TDR (April 30, 1997), excluding the overall support structures, and in the case of the pixel TDR, the B-layer thermal barrier.

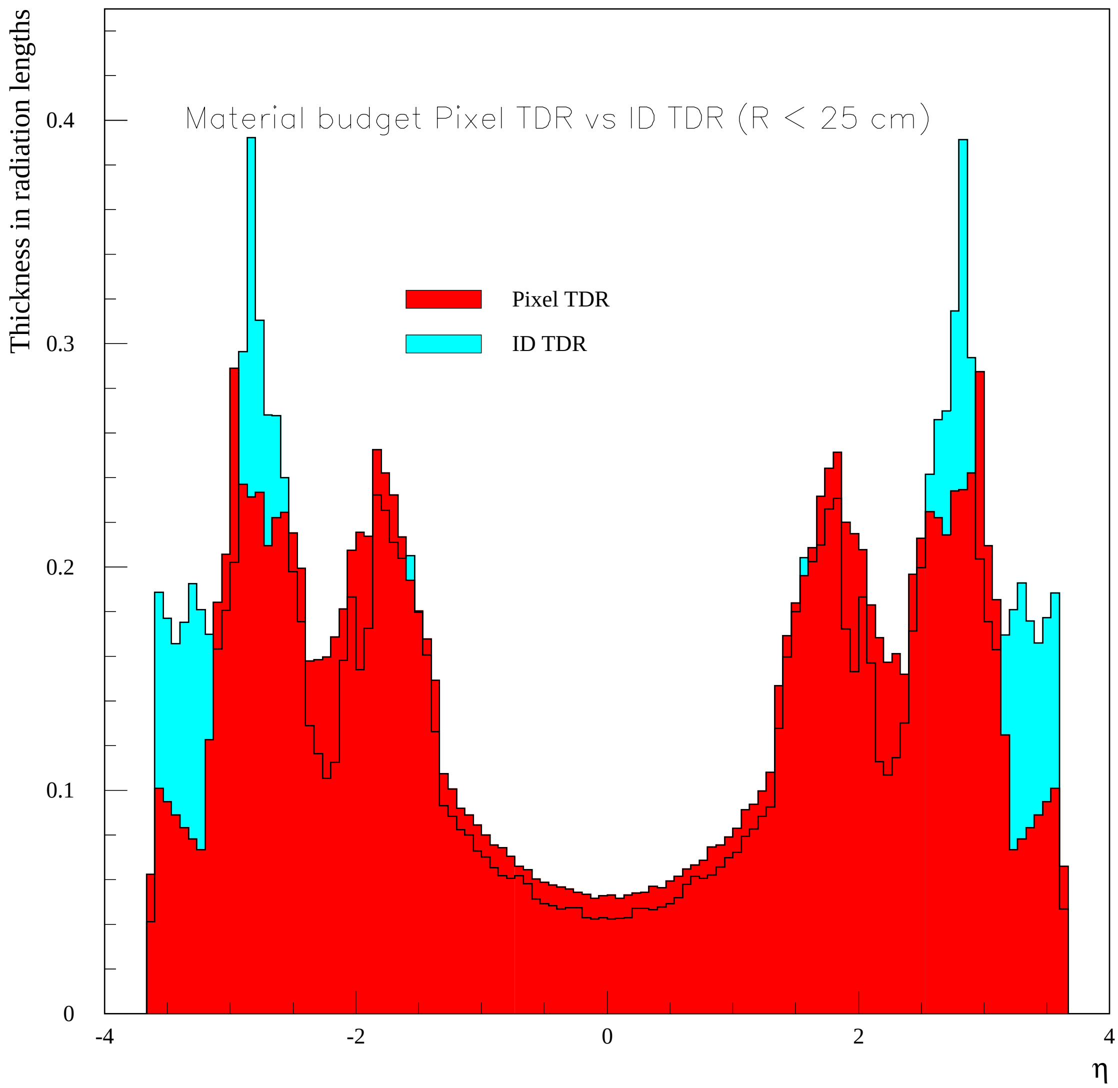

Figure 8-5 Total pixel material in radiation lengths in the current simulation and at the time of the Inner Detector TDR within the pixel volume (R<25 cm).

8.3 Pixel Module Material

An estimate of the material in a disk module with Al-kapton hybrids for interconnection is given in Table 8-3. This table shows a typical breakdown of the material in a module. Module options are compared in Section 8.6.

8.4 Mechanics Material

The material in a barrel stave of the “stepped” and “shingled” designs are given respectively in Table 8-4 and Table 8-5. In each case, the estimate for the material in radiation lengths is averaged over the dimensions 20.0 mm x 782.4 mm.

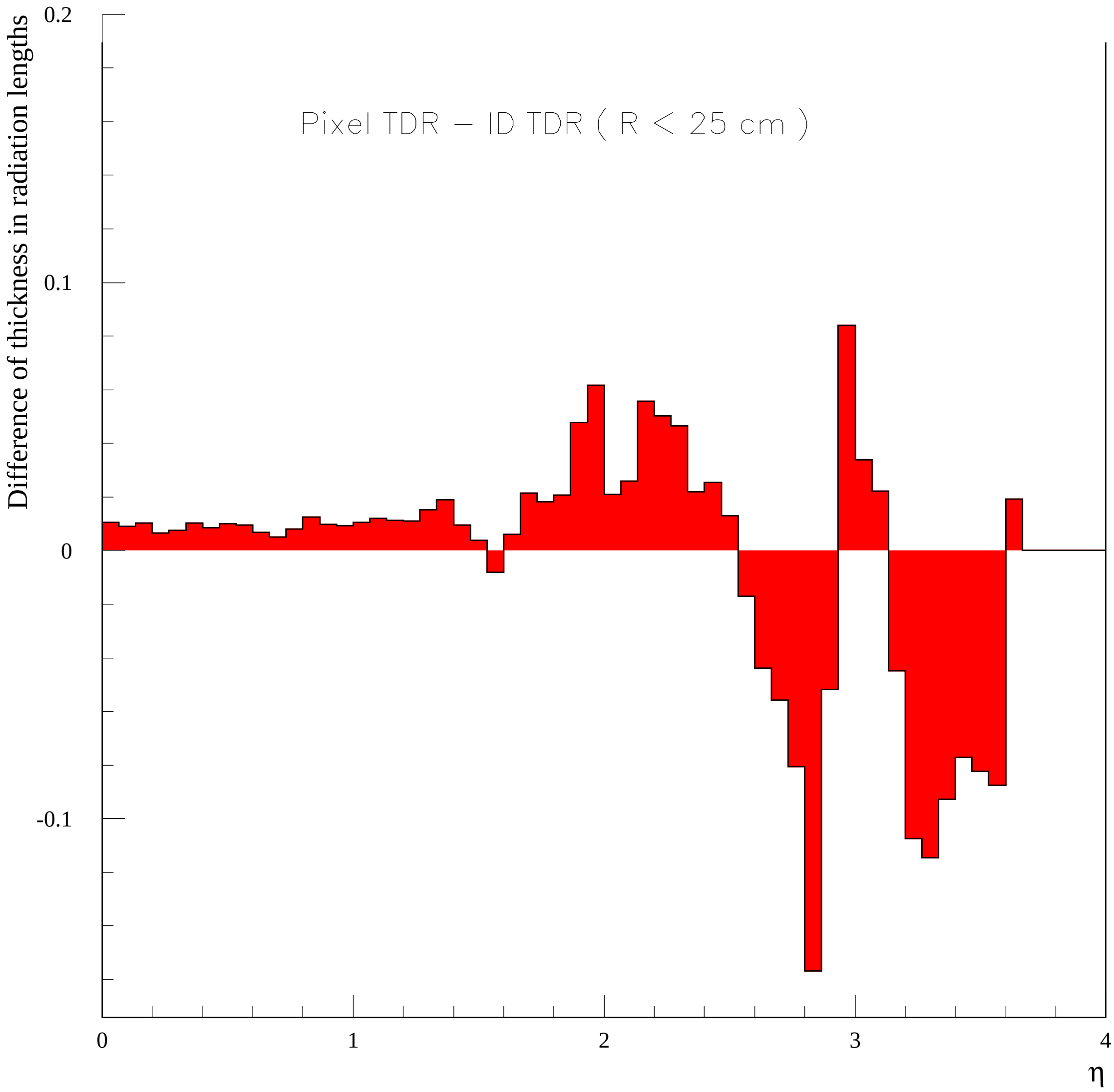

Figure 8-6 Difference in material in the pixel volume (R<25 cm) between the present estimates and those at the time of the Inner Detector Technical Design Report.

The material estimates for the ESLI (all-carbon), and the C-C + aluminium tube disk sector concepts are shown in Table 8-6.

The material in the supporting structures described in Chapter 7 of the pixel TDR is summarised in Table 8-7 and is estimated by averaging over the physical dimensions in each case for normal incidence.

Table 8-3 Material in a pixel disk module with aluminium-kapton hybrids.

Item	No. of	X(mm)	Y(mm)	Unit Area	Total Area	Thickness	X_0 mm	X_0 (%)
Chips	16	10.6	7.4	78.44	1255.04	0.15	93.6	0.151%
Bumps	61440	0.02	0.02	0.0004	24.576	0.02	10	0.004%
Detector	1	18.4	62.4	1148.16	1148.16	0.25	93.6	0.230%
Bias contact	1	2	2	4	4	0.025	14.3	0.001%
Bias cable kapton	1	1	10	10	10	0.05	284	0.000%
Bias cable cover	1	1	10	10	10	.0125	284	0.000%
Bias cable metal	1	1	10	10	10	0.007	14.3	0.000%
Bias cable adhesive	2	1	10	10	10	0.0125	250	0.000%
Flex wire bonds	416	3	0.025	0.075	31.2	0.025	89	0.001%
Flex glue	1	18.5	60.4	1117.4	1117.4	0.0125	250	0.004%
Flex passivation	1	18.5	60.4	1117.4	1117.4	0.0125	284	0.004%
Flex adhesive	1	18.5	60.4	1117.4	1117.4	0.0125	250	0.004%
Flex metal 1(50%)	1	18.5	60.4	1117.4	1117.4	0.007	89	0.003%
Flex kapton	1	18.5	60.4	1117.4	1117.4	0.05	284	0.015%
Flex metal 2(50%)	1	18.5	60.4	1117.4	1117.4	0.007	89	0.003%
Flex adhesive	1	18.5	60.4	1117.4	1117.4	0.0125	250	0.004%
Flex passivation	1	18.5	60.4	1117.4	1117.4	0.0125	284	0.004%
MCC	1	7	10	70	70	0.15	93.6	0.008%
MCC wire bonds	50	1	0.02	0.02	1	0.02	89	0.000%
Optical package	1	5	5	25	25	1	93.6	0.020%
Optical fibers	3	0.25	30	7.5	22.5	0.25	127	0.003%
Pigtail glue	1	6.8	10	68	68	0.0125	250	0.000%
Pigtail passivation	1	6.8	10	68	68	0.0125	284	0.000%
Pigtail adhesive	4	6.8	10	68	272	0.0125	250	0.001%
Pigtail metal 1(50%)	1	6.8	10	68	68	0.025	89	0.001%
Pigtail kapton	1	6.8	10	68	68	0.05	284	0.001%
Pigtail metal 2(50%)	1	6.8	10	68	68	0.025	89	0.001%
Pigtail passivation	1	6.8	10	68	68	0.0125	284	0.000%
Pigtail wire-bonds	25	1	0.025	0.025	0.625	0.025	89	0.000%
Ceramic capacitors	48	1	0.5	0.5	24	0.35	35	0.018%
Ceramic resistors	8	1	0.5	0.5	4	0.35	35	0.003%
Temperature sensors	1	1.6	1.2	1.92	1.92	0.4	35	0.002%
							TOTAL	0.485%

Table 8-4 Material estimate for a pixel barrel stave of the stepped (chips-down) design. All dimensions are in mm. The material is estimated averaging over an area given by 20.0x782.4 mm. Overlap is not included.

Item	No. of	X(mm)	Y(mm)	Unit Area	Total Area	Thickness	X_0 (mm)	X_0 (%)
Thin C-C(sealed)	1	20	782.4	15648	15648	0.4	224.5	0.178%
Thick C-C(sealed)	6	12	56.2	674.4	4046.4	0.6	224.5	0.069%
Glue for channel	1	5	782.4	3912	3912	0.1	120	0.021%
Channel support	1	14.8	782.4	11579.5	11579.5	0.3	202.5	0.110
Module glue/grease	13	20	60.18	1203.6	15646.8	0.05	120	0.042
Coolant(C4F10)	1	11.3	782.4	8841	8841	0.2	200	0.057%
							TOTAL	**0.476%**

Table 8-5 Material estimate for a pixel barrel stave of the shingled design with an aluminium cooling tube. All dimensions are in mm. The material is estimated averaging over an area given by 20.0x782.4 mm. Using a beryllium tube would make the total 0.556% X_0. These values do not include overlap.

Item	No. of	X(mm)	Y(mm)	Unit Area	Total Area	Thickness	X_0 (mm	X_0 (%)
Sloped tile	12	20	58.0	1160	13920	0.609	230	0.233%
Middle tile	1	20	51.5	1030	1030	0.972	230	0.028%
Glue for channel	1	2	784.4	1569	3137	0.1	120	0.017%
Channel support	1	18	784.4	14119	14119	0.3	202.5	0.132%
Module glue	13	20	60.18	1203.6	15646.8	0.05	120	0.041%
Coolant pipe	1	12.57	784.4	9860	9860	0.2	89	0.140%
Thermal grease	1	6.28	784.4	4926	4926	0.05	120	0.013%
Coolant(C4F10)	1	11.3	784.4	8864	8864	0.2	200	0.056
							TOTAL	0.661%

Table 8-6 Material in a pixel disk sector averaged over the active region.

Item	ESLI all carbon sector X_0 (%)	Aluminium tube sector X_0 (%)
Carbon-carbon faceplates (0.5 mm) thick	0.444	0.444
Adhesive for fill	0.035	0.024
Fiber or carbon foam fill	0.136	0.020
Coolant tube	0.093	0.180
Glue/grease for coolant tube	----	0.141
Coolant (C4F10)	0.020	0.020
TOTALS	0.729	0.830

Table 8-7 Material at normal incidence in the pixel supporting structures.

Item	X_0(%)
Thermal barrier	0.22
B-layer shell/support	0.32
1st layer shell/support	0.17
2nd layer shell/support	0.17
Disk support ring (each)	0.4
Disk spaceframe support	0.36
Barrel spaceframe support	0.2
End cones for barrel support	0.31

8.5 Pixel Sub-System Design Options

The estimated material, implemented in the current simulation, corresponds to a module design with aluminium-kapton hybrids (and power bus in the barrel region) and a “stepped (chips down)” stave design. A number of different designs are under investigation for the modules, barrel staves and disk sectors.

Some of the possible module designs are compared in Table 8-8. Barrel module designs with Al-kapton

Table 8-8 Comparison of material in $\%X_0$ in different pixel barrel and disk module concepts. The material is estimated by averaging over the physical area of 21.4 mm x 62.4 mm.

	Barrel Al-Kapton	Barrel Cu-Kapton	Barrel MCM-D Al-Kapton	Barrel MCM-D Cu-Kapton	Disk Al-Kapton	Disk Cu-Kapton
Detector substrate	0.230	0.230	0.290	0.290	0.230	0.230
Electronics +fibre-optics	0.199	0.199	0.199	0.199	0.182	0.182
Bumps+ wire bonds	0.004	0.004	0.004	0.004	0.004	0.004
Interconnect hybrids or MCM-D	0.091	0.198	0.118	0.207	0.046	0.087
Passive components	0.023	0.023	0.023	0.023	0.023	0.023
TOTALS	0.547	0.654	0.634	0.722	0.485	0.526

and Cu-kapton flex hybrids for interconnection and power distribution are compared to the MCM-D approach, assuming an identical Al-kapton hybrid for power bussing or individual Cu-kapton cables to provide the power connections. A similar comparison between Al-kapton and Cu-kapton hybrids for disk modules is also shown. The only essential difference between a barrel and disk module is in the power connections, which can be simpler in the case of a single annulus of disk modules rather than the more complicated distribution needed along the length of one-half of a stave.

In Table 8-9 the material in radiation lengths of some possible barrel and disk combinations are com-

Table 8-9 Comparison of material in radiation lengths of some combinations of pixel design options.

Design Combination	Radiation Length (% X_0)
Stepped stave/Al-kapton module	1.44
Stepped stave/Cu-kapton modules	1.59
Shingled stave/Be tube/chip-down modules (Al kapton)	1.55
Shingled stave/Be tube/MCM-D modules (Al kapton)	1.67
Shingled stave/Al tube/MCM-D modules (Al kapton)	1.81
Shingled stave/Al tube/MCM-D modules (Cu kapton)	1.94
Disk sector (0.75%)/Al-kapton module	1.55
Disk sector (0.75%)/Cu-kapton module	1.62
Disk sector (0.75%)/MCM-D modules (Al kapton)	1.75

pared. The material is calculated at normal incidence and takes into account overlap factors in azimuth and in z. In the case of the disks, we assume for the table an average radiation length of 0.75% for the thermo-mechanical structure. The material in services and supports will remain the same for all stave, sector and module options.

8.6 Possibilities for Material Reduction in the Pixel Sub-System

In general, there are now limited possibilities to consider that may result in a reduction of material below the level currently assumed in the simulation of the pixel system. There are three possible areas in which it may prove possible to reduce material, but additional investigations must be completed before accepting any of these possibilities:

Firstly, it may be possible to slightly thin the basic mechanical structure for staves and disks, at the risk of reduced mechanical rigidity and stability, and possibly impaired thermal performance. Additional prototype tests and finite-element calculations are required before accepting such a reduction. For example, in the case of the disk sectors, a reduction of the face-plate thickness to 0.3 mm from 0.5 mm would reduce the material in a sector by about 0.15% X_0; a ~ 20% reduction in the total sector material.

Secondly, the use of smaller cooling tubes or channels will be considered. The tube used so far in the prototype tests was originally sized for use of liquid (binary ice) cooling, and could possibly be reduced given the apparently superior cooling performance of the evaporative cooling. Since the coolant tube or channel, particularly in the barrel stave also provides rigidity, this would have to be carefully evaluated. Again prototype tests and calculations would have to be done before accepting this reduction, which would in any case only result in a < 0.1% X_0 saving.

Finally, the need for a thermal barrier (0.22% X_0 at normal incidence per layer) inboard of layer 2 and 3 and around the end-cap disk system, to allow safe removal and replacement of the B-layer for vacuum bake-out adds significant material, particularly in the disk region. If the B-layer removal and the insertion of the vacuum bake-out apparatus could be done rapidly, and the detector coolant restored within a day or few days, it might be possible to eliminate this barrier (or at least move it out toward the boundary radius between the pixel and SCT systems). In the pixel system, the effect on the detector depletion voltage for a day or few days of warm up to room temperature is negligible in the first few years of operation, and only begins to be appreciable after several years of operation at high luminosity. However, before deciding whether or not to implement the thermal barrier, a complete conceptual design of the B-layer insertion tooling is required, together with a detailed understanding of the consequences of installing the apparatus needed for the vacuum bake-out. This information should be available at the time of completion of the Technical Coordination Technical Design Report.

9 Services

The main change in the services since the TDR is the evaporative cooling system, already discussed. Other than this, the routings have changed. All of the end-cap SCT services now exit the TRT between wheels 14 and15. The change in the SCT end-cap services due to this rerouting is shown in Figure 9-1.

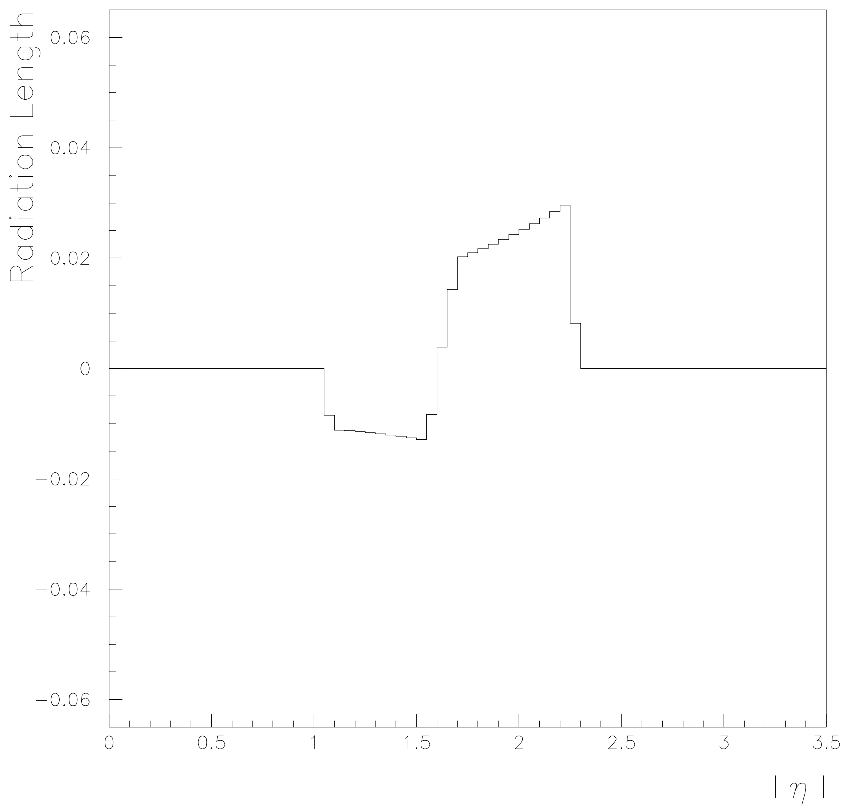

Figure 9-1 Change in material due to the rerouting of the SCT end-cap services.

The squirrel cage design was not complete at the time of the TDR. The contribution from this item is shown in the TRT section (1.55% X_0 at z=840-3200mm). The prototype is now under construction and it is planned to equip it with cables and a TRT module-0 element for tests. The results will be presented in the final ID engineering review.

A considerable effort has also been focussed on the patch panels PPB1 and PPF1 (see Figure 3-2) where the service disconnects are placed at the end of the barrel and end-cap detectors. Designs now under consideration use PEEK rather than metal for the bulkheads which support the connectors, and lower mass, high-pressure aluminium pipe fittings are being prototyped in industry to replace the stainless steel ones considered to date. An estimate of the reduction possible for the SCT only has been made and is included in the SCT tables. However the full design of the patch panel is needed before the full change can be estimated. At present, it appears that the designs of both patch panels can be improved significantly in material terms compared to the TDR estimates. These components will be validated by making full-scale models of the service paths in the barrel/end-cap crack, and in the end region of the ID where the services exit through the calorimeter. This will allow issues of access and maintenance to be addressed, and test the practicality of the connectors foreseen.

The ID material audit has made a considerable number of detailed proposals for material reduction in the services. These include:

- a change in the connectors for the SCT at PPB1, where 4224 connectors are implied by the TDR design, containing 168960 mm^3 of bronze, in low mass zero-insertion-force (ZIF) connectors. Proposals to reduce the number of connectors with custom-made designs, and to use smaller surface-mount connectors are under consideration;
- a reduction in the kapton thickness of the SCT low mass cables from 50 to 25 microns. This requires industrial R&D;
- the integration of the pixel and SCT opto-boards carrying the optical transmitters and receivers with the low mass cables;
- the suppression of connectors at PPF1 by making the cable breaks at PPF2. This implies long cable tails and a more complex installation and access procedure. An alternative under active consideration is to move components from PPF1 into the calorimeter gap. However, so far, no solution has been found in the available space;
- the use of PEEK rather than metal for pipe runs on the cryostat wall, other than those of the TRT ionisation gas, which would suffer from outgassing. The compatibility of PEEK with C_4F_{10} coolant is under study;
- the use of VCSELs for data transmission in the pixels, avoiding the need for metal data lines to the radius at which LEDs would survive. This is now the baseline;
- a reduction in the number of temperature sensors on the pixel detector.

The low-temperature operation of the SCT and pixel subsystems requires active thermal shields, cooled on the inner surface and heated on the outside to maintain the dry cold environment inside a thermally neutral boundary. The present estimates include disks of passive insulation between the barrel and end-cap regions, allowing separate extraction of the end-cap region without compromising the barrel, and a layer between the B-layer and pixel barrel 1 to avoid warming the pixel detector when the B-layer is extracted for beam-pipe bakeout operations. The bakeout scenario is under active study, to ascertain whether this layer can be dispensed with.

10 Conclusions

As the design of the ATLAS ID been finalised, the total material budget has remained stable, in spite of the inclusion of new items, such as provisions for the independent extraction of the B-layer.

11 References

11-1 Pixel System TDR (1998) LHCC 98-13

11-2 Inner Detector TDR, Vol. 2 (1997) LHCC 97-17.

11-3 D. Barberis et al., ATLAS Internal Note, INDET-No-188 (1997).

11-4 ATLAS Inner Detector Material: Comments and Future Directions (22 August 1997).

12 Appendix 1

Summary of InDet-No-188

A Comparative Study of Reduced Layouts of the Atlas Inner Detector

The performances of reduced Inner Detector layouts are compared to the performance of the full layout presented in the Inner Detector Technical Design Report. Three layouts have been fully simulated: a “new” TDR layout (“3+4”), with a material distribution as described in volume 2 of the ID TDR, a “new” layout with only 2 pixel layers (“2+4”) and one with only 3 SCT layers (“3+3”).

The most challenging pattern recognition study addressed in the ID TDR concerns the reconstruction and subsequent tagging of $H \rightarrow b\bar{b}$ and $H \rightarrow u\bar{u}$ with m_H = 400 GeV/c^2. This note reports on an update of that study with the reduced layouts, and on the consequences of degraded detector efficiency (90% instead of 97% in the precision layers) and pile-up at high luminosity. Reconstruction is performed with improved versions of the xKalman and iPatRec programs. Additional cuts are applied on track quality (impact parameter in R-z, χ^2/dof and number of shared hits) and improve R_u by up to 50% for all layouts and for both pattern recognition codes. The final analysis procedures are similar to those described in the ID TDR. The requirement on the minimum number of hits is reduced by the number of removed detector layers in the case of the reduced layouts and by one in the case of 90% efficiency.

Table 1 u-jet rejection for 50% b-jet efficiency.

layout	iPatRec	xKalman	xKalman ε=90%	xKalman pile-up
3+4	80±6	81±6	63±4	67±5
2+4	60±3	57±4	47±3	44±2
3+3	73±5	73±5	52±3	59±4

Table 1 shows R_u for the baseline and reduced layouts for the default (97%) efficiency, for 90% efficiency and with pile-up at high luminosity. A clear degradation is observed for the reduced layouts compared to the default setup, more pronounced for the “2+4” layout, mainly due to wrong associations in the pixel B-layer. In the “3+3” case, the degradation is mainly in the end-cap region. In the presence of a degradation of detector efficiency to 90% (which is quite plausible), the b-tagging performance of all layouts at low luminosity falls by ~25%.

If one takes the improved values of R_u (which reduce the sensitivity to the layout changes), it is possible to calculate the change in significance $S/\sqrt{B}$ and in the ratio $R_{red/irred}$ of reducible to irreducible background for the WH ($W \rightarrow l\nu, H \rightarrow b\bar{b}$) signal for an integrated luminosity of 3×10^4 pb^{-1}. In the “2+4” case the significance decreases by 6% and $R_{red/irred}$ increases by 25%, while in the “3+3” case the significance decreases by 2% and $R_{red/irred}$ increases by 10%. The performance is even worse in case of 90% efficiency or high luminosity. Other physics channels containing higher b-jet multiplicities ($t\bar{t}H$ with $H \rightarrow b\bar{b}$, SUSY physics) will obviously be even more strongly affected.

The outer SCT layers are important for reconstructing K^0_s’s, for example in $B^0_d \rightarrow J/\psi\, K^0_s$. At least two space points in the SCT are needed for K^0_s reconstruction; in the “3+3” layout this requirement reduces the maximum decay radius by 3.7 cm and results in an efficiency loss of at least 5% for the default detector efficiency.

The effects of reduced layouts on the Level-2 trigger rates have been studied for electron triggers. Removing a pixel or an SCT layer produces similar results: the efficiency can be maintained by lowering the minimum number of space points to 3, at the cost of a 40% increase in rate for the default detector efficiency; this degradation is avoided if the TRT is included.

The effect of reduced layouts on the EM calorimeter performance has been evaluated by looking at single electrons of E_T=10 GeV at η=1.2 (this is the worst case) and at the two most sensitive physics channels: $H \rightarrow \gamma\gamma$ (m_H=100 GeV/c^2) and $H \rightarrow ZZ^* \rightarrow 4e$ (m_H=130 GeV/c^2).

Table 2 Calorimeter performance for the baseline and reduced layouts.

layout	Tails (single electrons) E_T=10 GeV, η=1.2	$H \rightarrow \gamma\gamma$ relative $S/\sqrt{B}$	$H \rightarrow ZZ^* \rightarrow 4e$ Acc. in $\pm 2\sigma$ mass bin
3+4	19.2±0.6%	1	86.2±1.5%
2+4	16.1±0.6%	1.03	89.0±1.6%
3+3	15.6±0.5%	1.00	88.3±2.0%

Table 2 shows that the impact of the reduced layouts is larger for $H \rightarrow 4e$ than for $H \rightarrow \gamma\gamma$, due to the presence of low p_T electrons in the final state in the first case. Furthermore the “2+4” layout is the best from the point of view of the EM calorimeter performance (2-3% gain in significance for the two physics channels considered), as expected since this layout has less material at small radii than the other two.

In conclusion, it has been shown that both reduced layouts, while giving a slightly better Calorimeter performance, give a significantly degraded Inner Detector performance, compared to the baseline layout, for b-tagging (including the Higgs search, top and SUSY physics), K^0_s reconstruction and Level-2 triggering. In particular, the significance of the WH channel, already marginal, is reduced further. There will be serious degradations in the ID performance arising from the inevitable effects of reduced detector efficiency and pile-up. The Inner Detector Community believes that it is highly undesirable to incur additional and avoidable degradations arising from a reduced layout. The impact on the calorimeter performance is being addressed by seeking reductions in passive material, rather than in sensitive elements. The layout with 7 precision layers will give the best overall performance for ATLAS; we therefore recommend to keep it as the baseline layout.